Faculty of Natural Science and Technology
Department of Physics

MASTER'S THESIS FOR

STUD. TECHN.
SVEIN ÅSMUND SLUNGÅRD

Thesis started:	01.20.2007
Thesis submitted:	06.29.2007

DISCIPLINE: CONDENSED MATTER PHYSICS

Norsk tittel: *"Elektrisk felt-induserte strukturer og elektroreologi i lagdelte nanosilikater"*

English title: *"Electric Field Induced Structures and Electrorheology of Nano-Layered Silicates"*

This work has been carried out at the Complex Materials Group at Department of Physics NTNU, under the supervision of Jon Otto Fossum

---

Trondheim, 06.29.2007

Jon Otto Fossum

Responsible Supervisor

Professor at Department of Physics

Abstract

This Master thesis was an experimental study of the structure and resulting electrorheological (ER) behaviour of clays dispersed in melted paraffin wax or silicone oil. Four kinds of clay were used. Laponite RD, Alkyl Quaternary Ammonium Smectite (AQAS), laponite RD treated with the surfactant Cethyltrimethylammonium Bromide (CTAB) (similar to the AQAS) and Nickel-Fluorohectorite (NiFH).

Laponite RD was treated with CTAB to make it lipophilic. The finished clay showed behaviour throughout the various experiments which suggest some improved stability of the suspensions. However, the production method was not optimal and there is still large potensial for improvement. A better method was suggested and tested by Dr. B. Wang with positive results, but the industry fabricated lipophilic clay AQAS made the surface modification with CTAB redundant.

Pictures of the ER structure of clays were taken with optical microscopes, both for dispersions in silicone oil and paraffin. Some films of the dynamics were also recorded, where dynamics of the chain structure were observed. Pictures of laponite RD in paraffin were taken between crossed polarizers, where birefringence and anisotropy were evident.

In order to improve the stability of the ER suspensions, exposure to ultrasound was attempted. The reduction of the sedimentation rate, i.e. the total sedimentation, for AQAS in liquid paraffin was significant. The memory of ultrasound treatment was also present to some extent in the same samples after solidification and reheating of the paraffin. Similar tests with silicone oil showed a slight improvement. Ultrasound was also tested with respect to sedimentation times. It was found that AQAS samples in silicone oil sediments slowed after ultrasound treatment and that the effect was strongest for low temperature ultrasound treatment.

Clay samples with ER structures frozen in paraffin were investigated with small angle X-ray scattering (SAXS) and wide angle X-ray scattering (WAXS). In addition, ER effect of clays dispersed in silicone oil was investigated in situ with SAXS. The scattering data from clay samples in paraffin were found to be of little value for both SAXS and WAXS due to dominant scattering from the paraffin wax. Some trace of anisotropic scattering was found, but no conclusions could be made. It was found that the field influence impaired the crystalline structure of paraffin. Scattering from the oil samples showed anisotropic pattern, indicating a direction preference of the clay particles and thus present ER effect.

Samples of AQAS in paraffin were investigated with an atomic force microscope (AFM) in tapping mode. No evidence for ER structure was observed using AFM.

Preface

This thesis was written for the Master of Science degree in Physics (Sivilingeniør) at the Norwegian University of Science and Technology (NTNU). The work has been done at the Complex Materials Group at the Department of Physics.

The work on this master thesis has given insight into practical laboratory work through designing experimental setups and equipment, and through the sample preparations and data analysis. Valuable experience in experimental physics have been achieved through the use of different probes and techniques. All rheometrical experiments and CTAB clay production were performed in collaboration with Børge Aune Schjelderupsen. The thesis represents a continuation of preliminary experiments performed in the course TFY 4705 in the fall semester 2006.

I would like to acknowledge my supervisor Professor Jon Otto Fossum for valuable instructions, Dr. Ahmed Gmira for giving help and training on the AFM, Dr. Boaxiang Wang for help and collaboration and fellow students Børge Aune Schjelderupsen and Nils Ivar Ringdal for collaboration on various experiments. I would also acknowledge Arnolf Bjølstad and the staff at the Instrumental Workshop, and Arne Moholdt and the staff at the Electronic Workshop for repairing and adjusting my equipment when needed.

Trondheim June 29th 2007 Svein Åsmund Slungård

Contents

List of Figures

Chapter 1

Introduction

Electrorheological fluids are fluids which can switch from liquid to solid state within milliseconds when an electric field is applied, due to a major change in the viscosity. This is illustrated in Figure 1.1. The viscosity change arises from a polarization of suspended particles in the fluid. This ability to easily control the rigidity of a suspension is of great interest in fields like robotics, automotive and military industry [2], and generally, in every situation where a controllable viscosity is advantageous.

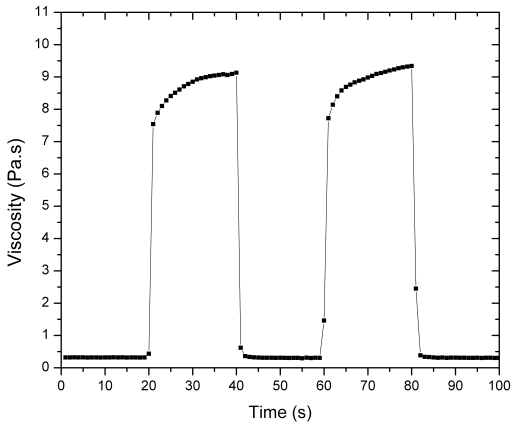

Figure 1.1: The viscosity of the clay suspension has an abrupt change in magnitude when a strong electric field is applied. The sample is sheared with a constant shear rate $\dot{\gamma} = 5\frac{1}{\mathrm{s}}$ with an electric field strength oscillating between 0 and $1\frac{\mathrm{kV}}{\mathrm{mm}}$.

Despite the huge potensial, several obstacles remains to overcome before ER devices can experience widespread commercialization. Three crucial problems with ER fluids today can be mentioned. A low yield stress, i.e. the strength of the chains, the lack of stability, i.e. the particle sedimentation over time, and a narrow operating temperature interval. [2, 3] Many questions are still unanswered and a better understanding of the underlying mechanisms are needed. It is thus a hope that this work can provide new knowledge to this scientific field.

The ER effect in the current work was created by placing the fluid between two conducting electodes. The fluid will then behave as an ER fluid when a strong electric field is present. This was achieved by applying a high voltage between the two electrodes, in accordance with the following equation:

$$E = \frac{V}{d}, \tag{1.1}$$

where V is the voltage and d is the distance between the electrodes.

The main objective for this thesis was to investigate the structure and resulting electrorheological behaviour of clays dispersed in melted paraffin wax or silicone oil. Several different investigative methods were used in the approach, where optical microscope, X-ray scattering and atomic force microscope constitute the main tools. Four different clays were used to prepare the ER fluids. Laponite RD, Alkyl Quaternary Ammonium Smectite (AQAS), laponite RD treated with the surfactant Cethyltrimethylammonium Bromide (CTAB) and Nickel-Fluorohectorite (NiFH).

To be able to disperse the laponite RD particles better, the surfactant CTAB was used to make laponite RD lipophilic. The goal was to prevent the particles from sedimenting, i.e. to stabilize the dispersion. AQAS is a fabricated lipophilic laponite clay, prepared with a surfactant similar to CTAB. Series of sedimentation experiments were performed to understand and reveal the sedimentation behaviour. Ultrasound treatment was tried as a method for improved stability. The goal was to increase the time of sedimentation and to reduce the total sedimentation, i.e. the amount of the particles which sediments over long time scales.

To better understand the ER structure, pictures of the samples were taken with optical microscopes, and some films of the ER development and dynamic were recorded. Paraffin samples were also examined with X-ray scattering and with atomic force microscope to learn more about the structures.

This thesis is split into five main parts. An overview of the underlying theories are described in part I. The equipment and compounds which were used are presented in part II. Part III consists of the experimental setups. Part IV describes and analysing the results, before the conclusion are presented in part V.

Part I

Theory

Chapter 2

Rheology

2.1 Introduction to Rheology

The term rheology was invented by Professor Bingham, and means *the study of the deformation and flow of matter*. [4] The definition was accepted in 1929 when the American Society of Rheology was founded. Rheology involves a wide range of scientific disciplines, and early papers included the study of materials such as asphalt, lubricants, paints, plastics and rubber. Nowadays the range is even wider with the introduction of biorheology, polymer rheology and suspension rheology. It is also important in the chemical process industry. [4]

2.2 Electrorheology

Materials that can undergo a phase-transition from liquid to solid-like state under the application of an external electric field, are termed (*positive*[1]) *electrorheological fluids* and were first described by W. M. Winslow [5] in 1949. The electrorheological fluid consists of finite-conductive polarizable particles in an insulating fluid, often an oil. The shear stress and viscosity of the fluid increases tremendously, often with several orders of magnitude, when field strengths in the order of 1 $\frac{\mathrm{kV}}{\mathrm{mm}}$ is applied. The solidification can occur within milliseconds when working with large fields. This behavior comes from a structural change of the suspended particles. When the field is applied, field-induced dipoles attract each other and tend to form chain structures in the direction of the field, as shown in Figure 2.1.

[1] If the viscosity of the dispersion increases under influence of an external electrical field, it is called a *positive* electrorheological fluid. If the viscosity decreases, the fluid is *negative* electrorheological [2]

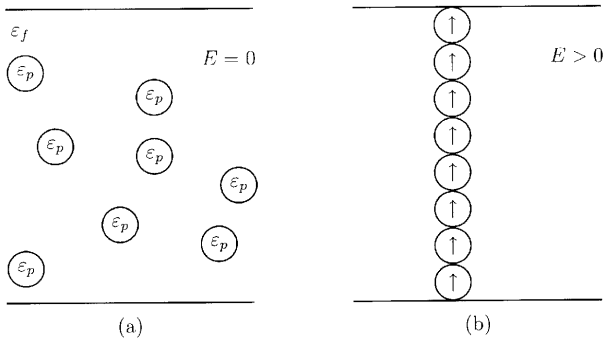

Figure 2.1: Electrorheological effect. (a) $E = 0$ and the particles in a liquid carrier are randomly oriented. (b) An electric field is applied and the particles are polarized and orients themselves in the direction of the field, forming chains and columns [6].

The chain structures restrains the fluid flow and therefore increase the viscosity and the shear stress. This effect is entirely reversible and the electrorheological (ER) effect will disappear and the fluid recover its original state within the same time-scale as it occurred when the electrical field is removed. This fast, strong and reversible change in the rheological properties provides a wide range of possible applications such as dampers, clutches, brakes, valves and actuators. Despite of this huge potential, few ER devices are available. This has to do with the lack of effective fluids [2, 7–10].

To achieve satisfying ER performance for an application, the fluids should fulfil several requirements where the most important are high dynamic yield stress, large increase in viscosity, fast response time, low current density through the fluid, stability against sedimentation, chemical degradation and irreversible flocculation. In addition, these fluids must also be able to operate over large temperature ranges. The complexity of the behavior of the fluid is also a problem in the design of ER devices. It is dependent of variables such as electric field strength and frequency, deformation history, temperature and composition. In addition, the solution often includes additives like surfactants and activators to improve the ER effect, complicating the situation even further [9, 10].

2.2.1 The Polarization Model

Electrostatic polarization models can describe many experimentally observed features of the ER fluids, such as the formation of aggregates and field strength and concentration dependence of formation properties. The agreements between observations and models suggest that polarization interaction between particles is the origin of the ER effect [10].

The polarization can be described using a simplified model based on identical spherical dielectric particles dispersed in an insulating fluid. Responses are assumed to be linear. Under the application of an electric field, each particle in the fluid is polarized, see Figure 2.1. The induced dipole moment is given by

$$\mathbf{p} = \frac{\epsilon_p - \epsilon_f}{\epsilon_p + 2\epsilon_f} \epsilon_f a^3 \mathbf{E}_{\text{loc}}, \tag{2.1}$$

where a is the radius of the spherical particle. ϵ_p and ϵ_f are the dielectric constant for the particles and fluid, and $\mathbf{E}_{\text{loc}}$ is the local electric field. The polarization is caused by a mismatch in the dielectric constants [6]. Equation (2.1) indicates that particles with large ϵ_p provides the strongest ER effect. This is not always the case, and demonstrates that the polarization model approach not always is sufficient. The model can not explain phenomena like the dependence of the electrical field frequency or the dependence of particle conductivity. The conductivity can be included in the polarization model by replacing ϵ with the complex permittivity. Such a model can describe the observed physics better than the simple polarization model, but the drawback of both methods are the lack of prediction for dynamic systems, i.e. they only apply after the microstructure has fully formed [11].

There exist more advanced and powerful models which can describe the observed physics better, e.g. a model by Khusid and Acrivos [12]. For a more complete understanding of the electrorheological theory, the PhD thesis by Huang [6] can be read.

2.3 The Shear-dependent Viscosity

The term viscosity describes a fluid's resistance to flow. Newton postulated[2] a linear relation between a shear stress τ and a velocity gradient, or shear rate $\dot{\gamma}$,

$$\tau = \eta\dot{\gamma}, \tag{2.2}$$

where η is the viscosity. For such liquids, called Newtonian fluids, the viscosity is independent of the shear rate. In rheology, most fluids do not show such behaviour, meaning that η is a function of the shear rate, $\eta(\dot{\gamma})$, often called the shear viscosity. Such fluids are called Non-Newtonian. Fluids with a viscosity which decreases with increasing shear rate are called shear-thinning fluids. Fluids with the opposite behavior are called shear-thickening. Suspensions and emulsions are typically Non-Newtonian fluids. [4] The viscosity is also strongly temperature dependent. The viscosity for Newtonian fluids decreases for increasing temperature, approximately according to the relation

[2] Philosophiae Naturalis Principia Mathematica (1687)

$$\eta = Ae^{\frac{-B}{T}}, \tag{2.3}$$

where A and B are fluid dependent constants. In general, the greater the viscosity, the stronger is the temperature dependence. [4]

Figure 2.2 shows the difference in shear response for Newtonian, shear-thinning, shear-thickening and Bingham fluids.

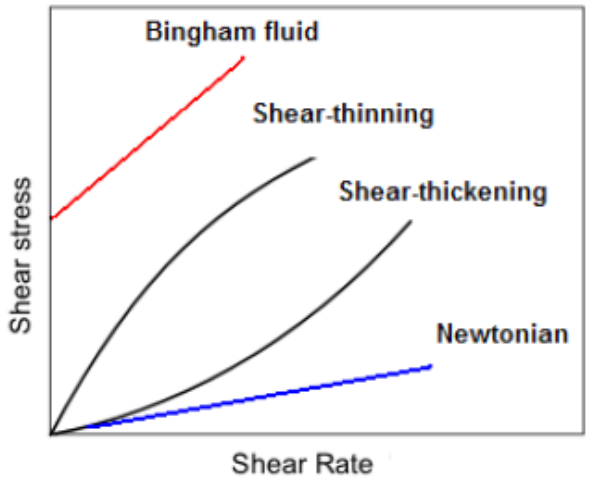

Figure 2.2: The relation between shear stress and shear rate for different fluids.

2.3.1 Bingham Fluids

Bingham fluids are Non-Newtonian fluids characterized by a yield stress. As opposed to newtonian fluids they can transmit a velocity gradient without a shear stress. To make a Bingham fluid flow, one must have a shear stress larger than the yield stress, which means that for shear stresses below this limit, the fluid will behave like a solid, and above the limit, as a fluid [13]. The electrorheological shear-response is commonly described with the Bingham model. The shear-stress τ is described as

$$\tau(\dot{\gamma}, E_0) = \tau_0(E_0) + \eta_{pl}\dot{\gamma}, \tag{2.4}$$

for $\tau > \tau_0$. $\dot{\gamma} = 0$ for $\tau < \tau_0$. Here, E_0 is the applied electrical field, $\dot{\gamma}$ is the shear rate, τ_0 is the dynamic yield stress and η_{pl} is the plastic viscosity [10]. The plastic viscosity will in general decrease with increasing shear rate, approaching

the zero field viscosity for high shear rates. This shear-thinning behaviour can be explained by chains or columns in the ER suspension which are gradually broken down by the increasing shearing. The yield stress τ_0 is found theoretically and experimentally to follow the relation

$$\tau_0(E_0) \propto \Phi^{\Delta} E_0^{\alpha}, \tag{2.5}$$

where Φ is the volume fraction of particles. The polarization model predicts that $\Delta = 1$ and $\alpha = 2$ [11]. For low and moderate field strengths it is observed $\alpha \approx 2$. For high fields, the magnitude of α decreases somewhat [10].

Chapter 3

Surface Treatment

3.1 Surfactant

Surfactants are usually organic amphiphilic molecules. The term amphiphilic means that the molecule has one hydrophilic part, usually called the "head", and one hydrophobic part, often a long hydrocarbon chain, usually called the "tail". This amphiphilic nature makes the molecule soluble in both water and organic solutions. The CTAB molecule shown in Figure 7.8 in chapter 7, shows a typically example of such an amphiphilic surfactant, with the characteristic "head & tail" design. When present in a solution over a certain concentration, the surfactant molecules aspire to make micelles. A micelle is an aggregate of surfactant molecules, where the molecules tends to minimize the contact between water and the hydrophobic part by encircling the hydrophobic tails with the heads. If the surfactant is solved in organic material, in this case oil or paraffin, the hydrophilic parts will be in the core, and the micelle is said to be reverse, shown in Figure 3.1 [14].

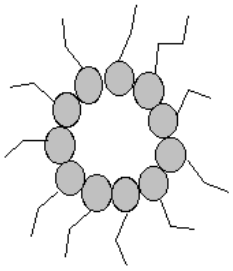

Figure 3.1: Schematic of a reverse micelle, showing the hydrocarbon chains creating a protecting shell around the hydrophilic parts.

3.2 Quaternary Ammonium Cation

The quaternary ammonium (QA) cation is a positively charged ion of the structure NR_4^+, where the Rs are alkyl groups. These alkyl groups can be different in size and even connected. Unlike regular ammonium ions, the QA is permanently charged, at any pH. These ions, or actually salts of this ion, can be used as surfactants [15], in our case, to modify the surface of clays. The CTAB (see section 3.3 and 7.3) is such a QA salt. The already modified clay, Alkyl Quaternary Ammonium Smectite (AQAS), see section 7.1.1, is modified with a QA surfactant to become lipophilic[1].

When a quaternary ammonium surfactant is added to a water/clay solution the charge balancing cations (Na^+ for laponite RD) on the clay surfaces will be exchanged by QA^+-ions. (In this case by CTA^+-ions) This is because of the propensity of the ions and the fact that the hydrophobic tail prefers to hide from the aqueous medium. If the amount of QA^+-ions present in the solution is right, a complete cation exchange is possible.

3.3 Ionic Exchange

Ion exchange is a reversible process where dissolved ions are taken up by a solid, replacing ions already attached to the solid. The amount of charge does not change neither in the solution nor on the solid in this process [17]. The property of adsorbing and absorbing ions in a solution is called *cationic exchange capacity*, CEC. This is a measure of the total number of charged ions which can be fixed onto the surfaces of clays, more specific the number of moles of ionic charge fixed on 100 g dry clay. The unit of the CEC is $\frac{\text{milli}-\text{equivalents}}{100\,\text{g}}$ or $\frac{\text{meq}}{100\,\text{g}}$. If ions or charged molecules in a solution can be attracted to a clay surface there will be a selection between the species available. The more there exist of a charged species in the solution, the more of it will be fixed on the clay surface, according to the law of chemical mass action. Some species are more strongly attracted to the clay than other. The selection depends on the constitution and species of clay and the affinity of the charged particles to remain in the solution. The preference for an species of ions to be taken up by the clay over another ion species, is called cation selectivity. If an ion is held on the clay surface and become displaced by another due to change in its aqueous concentration, the ion is desorbed. If it is desorbed by an ion introduced by the aqueous solution, it is said to be exchanged [18].

[1] Lipophilic materials are materials which attract non-polar organic compounds, most notably oils, fats, greases, and oily substances. In most cases, synonymous with hydrophobic [16].

Chapter 4

X-ray Scattering

Among the probes that can be used to investigate the structure of condensed matter, scattering experiments are of particular importance due to their applicability. The source of information is usually electromagnetic waves, (in addition to neutrons and electrons) where X-rays, waves in the range 0.01 - 10 nm, were used in the current experiments. The setup is characterized by a primary beam with frequency ω_0, a wavevector $\vec{k}$ and an intensity I_0. The waves hit the sample and creates spherical scattering waves. The resulting scattered intensity I depends on the observation direction and the sample-detector distance R. [19]

The terms scattering and diffraction are closely related to each other. In optics, scattering is defined as interaction of waves or photons with unordered atoms, while diffraction is described as scattering in those situations where some of the object is made up of ordered atoms. These arranged atoms scatter the waves in spesific directions. A single atom scatter an incident X-ray beam in all direction in space, but when the number of atoms are large and arranged in a periodic lattice they scatter, or diffract, the beam in relatively few directions. This happens because the periodic arrangement of atoms or ions causes destructive interference in all directions except for those predicted by Bragg's law, where contructive interference occurs. When the crystal contains imperfections, the diffraction occurs at non-Bragg angles so that the Bragg peaks are no longer delta-functions. [11]

The Bragg scattering law provides information on the arrangement of atoms in crystalline structure materials. This scattering can be periodic, originated from crystalline nature, or non-periodic, from disordered nature. The scattered intensity I is often described as a function of the scattering vector $\vec{q}$, which is given by

$$\vec{q} = \frac{4\pi}{\lambda} \sin\left(\frac{2\theta}{2}\right), \tag{4.1}$$

where λ is wavelength and 2θ is the scattering angle, the angle between the scattered and transmitted beams. For constructive interference of scattered X-rays, Bragg's law is given by

$$2d_{\mathrm{hkl}} \sin\left(\frac{2\theta}{2}\right) = n\lambda, \tag{4.2}$$

where d_{hkl} is the spacing between any two hkl planes of the crystal. Bragg reflections can occur only for wavelengths $\lambda \leq 2d_{\mathrm{hkl}}$. These equations are based on and derived for ideal conditions. The principle of Bragg scattering is shown in Figure 4.1. Bragg's law is a purely geometrical law.

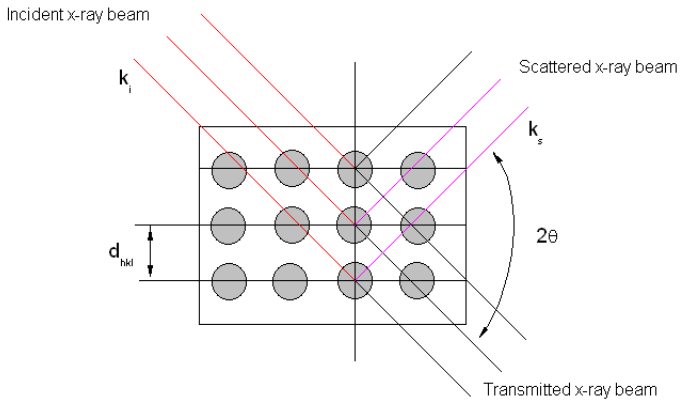

Figure 4.1: The principle of Bragg scattering. k_i and k_s are the incident and the scattered wave vector. The relationship between them is $\vec{q} = \vec{k}_s - \vec{k}_i$. The path difference is $2d\sin(\theta)$.

Comparing equation 4.1 and 4.2 leads to

$$q_{\mathrm{hkl}} = \frac{2\pi}{d_{\mathrm{hkl}}}. \tag{4.3}$$

When combining these equations it is easy to determine the spacing d between any two of the crystalline planes.

It is the scattered intensity which is measured by the detector. There are many ways of describing this intensity. According to Strobl [19], it is in general given by

$$I(\vec{q}) \propto \left\langle |E_0'(\vec{q})|^2 \right\rangle \propto \sum_{j,k} f_j f_k \left\langle e^{-i\vec{q}(\vec{r_j} - \vec{r_k})} \right\rangle. \tag{4.4}$$

where E_0 represent the amplitude of the scattered wave, f_j and f_k are form factors and $\left\langle e^{-i\vec{q}(\vec{r_j}-\vec{r_k})} \right\rangle$ are a phase term.

Powder Scattering

Different materials scatter X-rays in different ways. A good crystalline powder, e.g. clay, consists of thousands of tiny crystallites oriented at random. The powder is isotropically distributed in three dimensions. Some of the particles have the correct orientation relative to the incident wavevectors $\vec{k_i}$, for Bragg scattering. The scattered wavevectors $\vec{k_s}$ are thus distributed evenly on a cone with $\vec{k_s}$ as the axis and an apex half angle 2θ. This phenomenon can be seen as the characteristic rings on the scattering data figures in chapter 15.

A thorough presentation of the scattering theory will not be presented, since much of it has little direct impact on the data analysis. A detailed theory presentation is easy accessible, and can be found in e.g. Strobl [19] or Nielsen and McMorrow [20].

Chapter 5

Optics

In optical microscopy, light is the source of information. Light can be described as transverse electromagnetic waves consisting of mutually perpendicular electric and magnetic fields, as shown in Figure 5.1. The propagation direction is perpendicular to both the magnetic and electric field such that the two fields and the propagation direction forms a right-hand system.

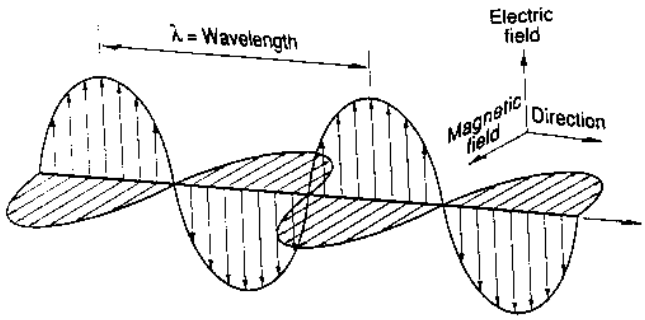

Figure 5.1: An elctromagnetic wave. [21]

5.1 Polarization

Polarized light is light where the electric field of all waves oscillates in a spesific direction. Materials which allows only light with a specific angle of vibration to pass through are called polarizers. If the light oscillates in a plane it is said to be linear polarized. If two polarizers are set up in series with parallel optical axes, light passes through both. However, if the axes are set up 90° apart (crossed), the polarized light transmitted through the first is extinguished by the second.

As the angle rotates from 0 to 90°, the amount of light that is transmitted decreases continuously until the polarizers absorbs everything at 90°. [22] This is shown in Figure 5.2.

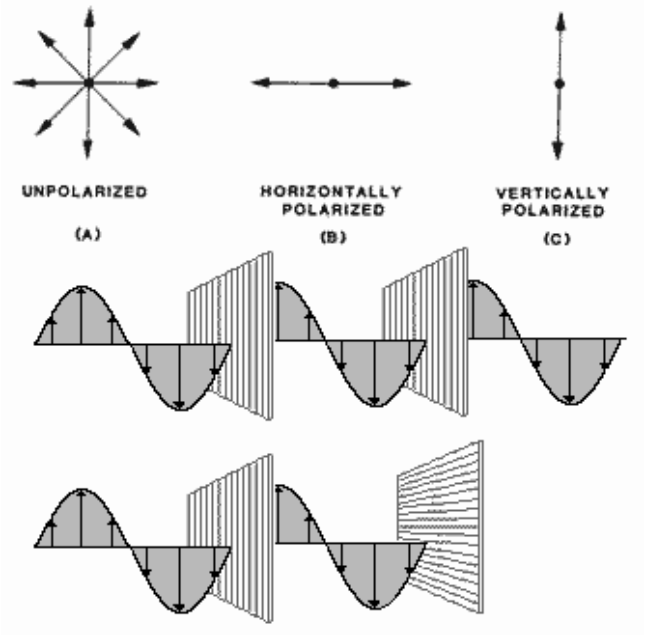

Figure 5.2: Linear polarization of light. Two polarizers are set up in series with parallel optical axes and light passes through both. Then the axes are set up 90° apart (crossed), and the polarized light transmitted through the first is extinguished by the second. [22]

5.1.1 Polarization Types

Consider two plane-polarized waves with a phase difference Φ.

$$E_x = A_x e^{i\omega t} \tag{5.1}$$

and

$$E_z = A_z e^{i(\omega t + \Phi)}, \tag{5.2}$$

where A_x and A_z are amplitudes, ω is frequency and t time. The light is in general elliptically polarized because the electric field vector describes an ellipse during each period of the wave. [23] If the amplitudes are equal, $A_x = A_z$ and $\Phi = 0$, these waves are in phase, and their vector sum leads to a linearly polarized wave at 45°, as shown in Figure 5.3 (a). Similarly, if Φ is π, the

resultant is linearly polarized at -45°, as shown in Figure 5.3 (b). If Φ is $\frac{\pi}{2}$, the ellipse becomes a circle if $A_x = A_z$, and the light is circularly polarized, as shown in Figure 5.3 (c). If the amplitudes (A) are equal but the phase difference Φ is a random variable of time, the light is unpolarized. Natural light such as sunlight or blackbody radiation is unpolarized or nearly unpolarized. [23–25]

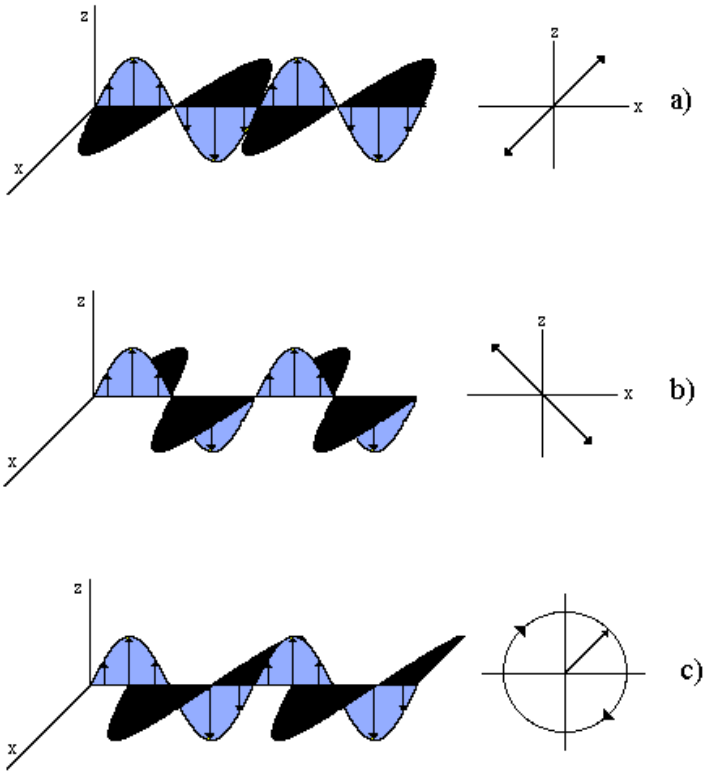

Figure 5.3: Different polarization directions of light. (a) If these waves are in phase, their vector sum leads to a linearly polarized wave at 45°, (b) Similarly, if the phase difference is π, the resultant is linearly polarized at -45°, (c) If the phase difference is $\frac{\pi}{2}$, the light is circularly polarized. [25]

5.1.2 Birefringence

Birefringent materials are materials that produces polarized light. They have two indices of refraction so that the incoming light can be separated into two waves. The refractive index n is given by

$$n = \frac{c}{v}, \tag{5.3}$$

where c is the vacuum velocity of light. This means that a difference in refractive index leads to differet velocities v, thus leading to a phase difference dependent on the transmitted material. This phase difference will introduce a change in polarization. [24] Some crystals are anisotropic, meaning that the physical properties vary with direction, e.g. the index of refraction. These materials are birefringent, which means that some light will transmit when they are placed between crossed polarizers. [23, 25] Pictures of birefrigent materials show distingusihed areas with different colours depending on the length and orientation of the birefringent material. The chain formations in ER materials give anisotropic particle distributions, and an investigation of such samples should lead to light transmittance. With no present ER effect, these samples could ideally be isotropic and not transmitting any light.

Part II

Equipment & Chemical Compounds

Chapter 6

Equipment

6.1 The Sample Cell

To make samples of frozen laponite chains, the cell shown in Figure 6.1 was used. The dispersed laponite was poured onto the cell which was placed on a piece of glass. When the paraffin is cold, the voltage can be turned off and the sample taken out from the cell for observation.

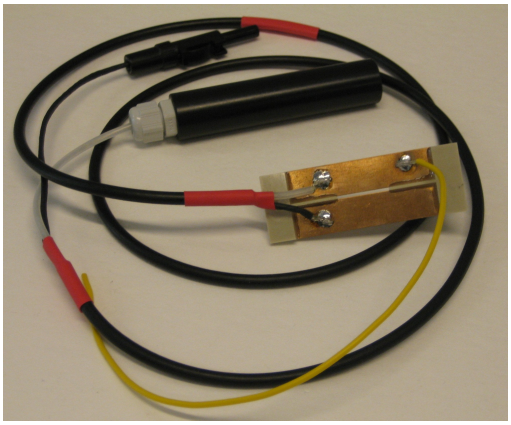

Figure 6.1: The sample cell. The sample is placed in the 1 mm gap between the two electrodes. The long black pipe is the high voltage contact. The small black contact is the ground contact. The yellow cable is placed on the cell to measure the actual voltage applied.

The cells were created particularly for these experiments, based on an old, similar model. The old model had a glass disk glued on beneath the electrodes, and this new model was designed with the same intention. Later, it was concluded

that it was much easier to remove the finished sample without the the glass disk. The absence of the glass lead to very fragile cells because of the very small areas where glue can be placed, and the cells needed repairs several times. In future experiments the cells should be redesigned to be more robust.

6.2 High Voltage Power-Supply

To achieve the required voltage needed in the experiments a high voltage power-supply was used, shown in Figure 6.2. The in- and out-voltage is proportional where $V_{in} = 0 - 15$ V and $V_{out} = 0 - 5\,k$V. All experiments were performed at $V_{out} = 2\,k$V.

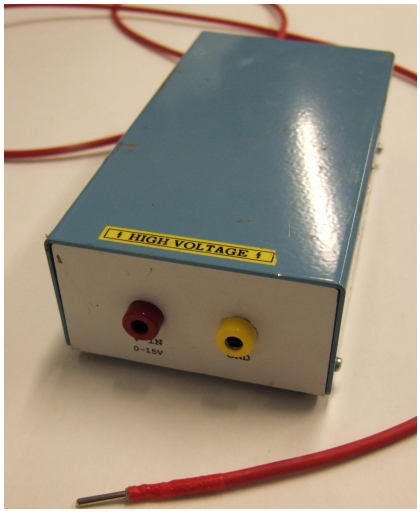

Figure 6.2: High voltage power-supply.

6.3 Optical Microscope

To observe and study the samples, an optical microscope, Zeiss Stemi 2000C Stereomicroscope, was used, shown in Figure 6.3.

To achieve additional magnification a 2x supplementary lens, screwed to the objective front lens mount, was available. This supplementary lens was more or less permanently mounted due to one of the light sources, Figure 6.6 (a), which was almost unattachable without the supplementary lens. To handle the samples on the microscope a very simple stage was used, shown in Figure 6.3 (b).

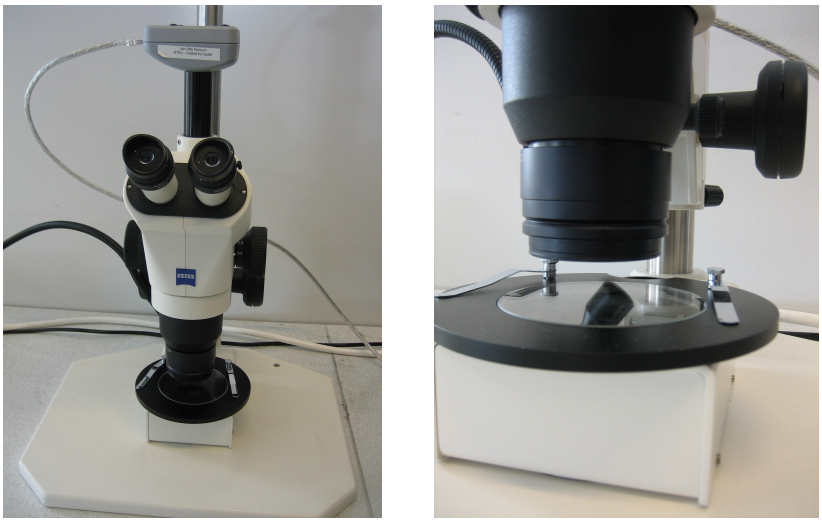

(a) (b)

Figure 6.3: (a): The microscope, (b): Close view showing the stage and the supplementary lens

6.4 Camera

One of the advantages of the microscope used is the camera port which allows a camera to be mounted on top of the microscope, and hence lets the user utilize a computer monitor for study instead of the eyepieces, which simplify the sample viewing considerably. The camera model used was a PixeLINK 1.3 Megapixel FireWire Camera PL-A642 (shown in Figure 6.4).

Figure 6.4: The camera [26].

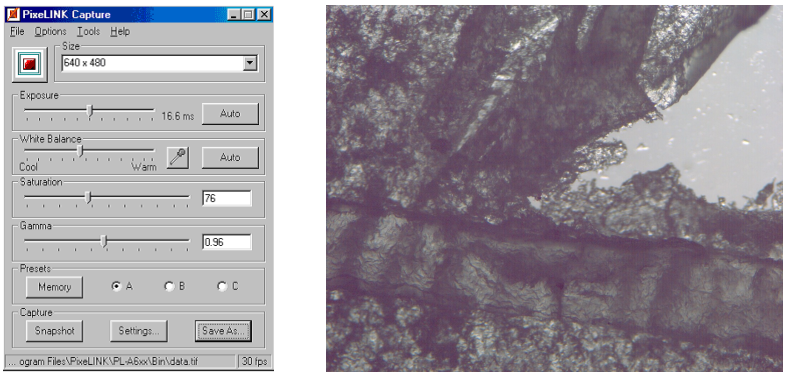

(a) (b)

Figure 6.5: (a): The software menu, (b): A captured picture of laponite in paraffin. The heigth of the picture is approximately 4.5 mm.

The camera is connected to the computer with a fire-wire cable. Software included with the camera offers real-time isochronous video streaming and makes it possible to follow the sample continuously, also under movement. The software gives the opportunity to adjust, e.g., the exposure and saturation of the image, but the perhaps greatest advantage of the camera compared to the eyepieces, is the option to take snapshot images of the sample at any time and setting [26]. The software menu and an example of a captured picture are shown in Figure 6.5 The camera was also used for making movies of the electrorheological dynamics, using Windows Movie Maker software.

6.5 Light Sources

To observe the samples in the microscope, two different light sources were used. One source, StockerYale 20, illuminates from above, and another, Zeiss KL 200, illuminates from beneath. The light sources are shown in Figure 6.6 (a) and (b), respectively.

6.6 Heating Plate

The heating plate, Heidolph MR3001, shown in Figure 6.7 offers a stepless temperature control and a stepless blender function. This is mainly used to heat the cell and glass plate before use. The purpose of the heating is to prepare the liquid paraffin without having to worry about solidification. It is also used as a blender and heater under the preparation of laponite with CTAB.

(a)

(b)

Figure 6.6: (a): The light source used to illuminate the samples from above, (b): The light source used to illuminate the samples from beneath.

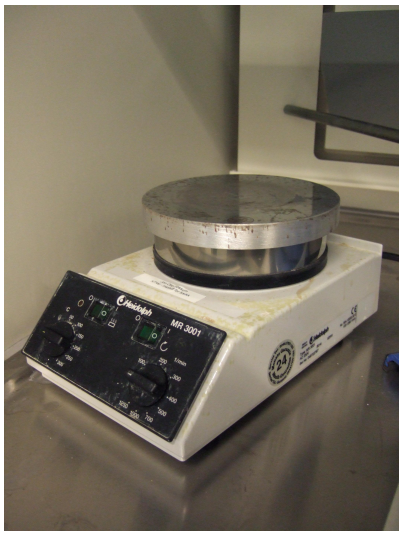

Figure 6.7: The heating plate.

6.7 Multimeter

The multimeter, PeakTech 4370, was used to measure the applied voltage over the cell. The multimeter is shown in Fig 6.8.

Figure 6.8: The multimeter. [27]

6.8 Voltage Divider

To be able to measure the applied voltage with a normal multimeter, a voltage divider was used. This is shown in Figure 6.9. The voltage is divided by a factor of 1000.

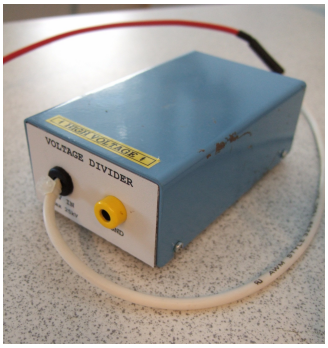

Figure 6.9: The voltage divider.

6.9 Ultrasonic Cleaner

The ultrasonic cleaner, a Branson 5510, was used to improve the dispersion of the clay solutions. It also has the possibility to be used as a heater. The cleaner is shown in Figure 6.10.

Figure 6.10: The Ultrasonic Cleaner. [28]

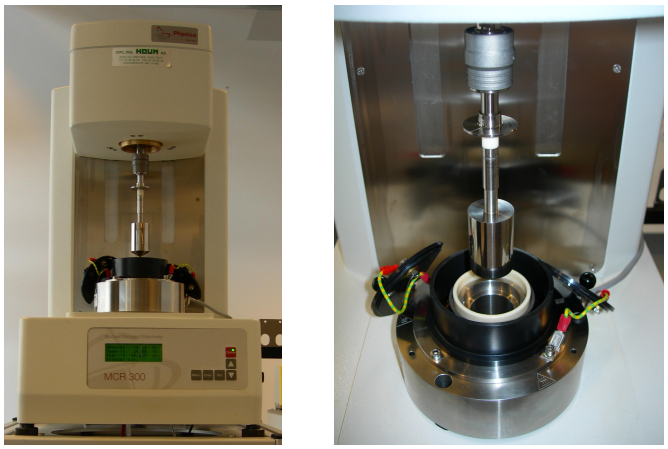

(a) (b)

Figure 6.11: (a): The rheometer, (b): The ERD-system

6.10 Rheometer

The rheometer used is a Physica MCR 300, shown in Figure 6.11. It is a rotational rheometer with an air bearing motor. The sample temperature can be controlled in a wide temperature range, limited by the heating liquid, in this case water. For electrorheological measurements the Electro Rheological Device (ERD) is used. It consists of a rotating concentric cylinder and a cup coupled to a high voltage supply. Voltages from 0 to 12.5 kV can be applied. The gap between the inner and the outer cylinder is 1.13 mm and the cup contains 19.35 ml sample.

6.11 Atomic Force Microscope

Scanning Probe Microscopy (SPM) consist of a family of microscopy forms where a sharp probe is scanned across a surface and some probe-sample interaction or interactions are monitored. The Atomic Force Microscopy (AFM) is one of two primary forms of SPM. The AFM has 3 different scans meodes, i.e. Contact mode, Non-contact mode and Tapping mode. In the current experiments the tapping mode was used, due to its superiority on soft materials (paraffin) scans. The force and hence the damage to soft surfaces is low. The only inconvenience with the tapping mode is that it is time-consuming compared to the other alternatives. [29] The AFM used is shown in Figure 6.12.

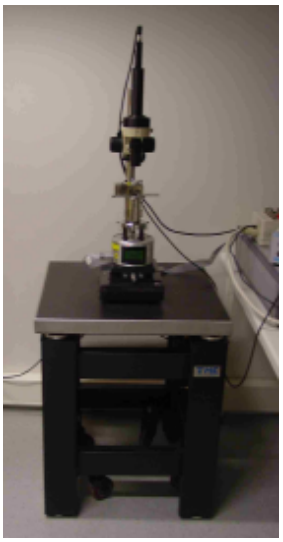

Figure 6.12: The Veeco MMAFMLN-AM multimode Atomic Force Microscope.

An overview of the tapping mode is shown in Figure 6.13. The microscope operates by scanning a tip attached to the end of an oscillating cantilever across the sample surface. The cantilever is oscillated with an amplitude ranging typically between 20 and 100 nm. The tip lightly "taps" on the sample surface during scanning, making contact with the surface at the bottom of its swing. The vertical position of the scanner at each data point in order to maintain a constant setpoint amplitude is stored by the computer to form a topographic image of the sample surface. [29]

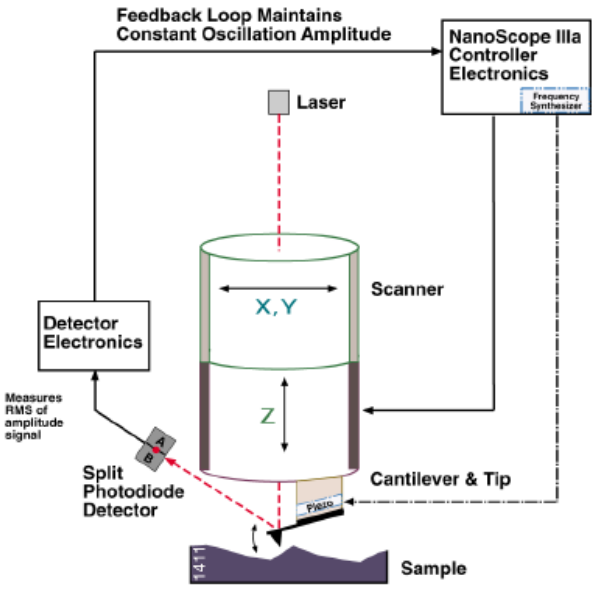

Figure 6.13: Schematic of the tapping mode AFM. [29]

6.12 SAXS

The X-ray scattering experiments were performed utilizing Bruker AXS NanoSTAR, a Small Angle X-ray Scattering (SAXS) system, shown in Figure 6.14. It uses a two dimensional detector and has the possibility of different sample-detector distances, hence making it possible to perform both SAXS and WAXS[1] experiments with the same equipment. The equipment consists of four main parts viz. the generating source, the pinhole collimating system, the sample chamber and the detector. The first two parts, the generating source and the pinhole collimating system, constitute an optical system that provides the X-ray beam to be monochromatic and well collimated.

The generating source is a water cooled rotating Cu anode. A crossed coupled monochromater, called Göbel mirrors, shown in Figure 6.15, selects the characteristic K_α radiation from the continuous white spectrum. The original divergent beam is adjusted to a two-dimensional parallel beam. [30]

The three pinhole collimation system, shown in Figure 6.16, limits the divergence and shadows the edge scattering of the system. The outcome from the first two parts of the NanoStar is a well defined, parallel and monochromatic X-ray beam. [30] The size of the point focus is 0.4 mm×0.8 mm, and the wavelength of the beam is $\lambda = 1.541838$ Å.

[1] Wide Angle X-ray Scattering

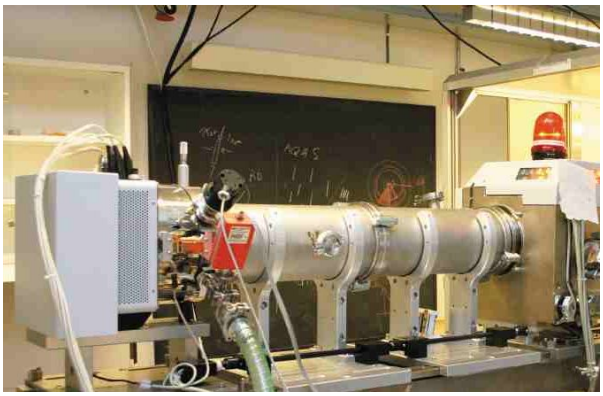

Figure 6.14: The Bruker AXS NanoSTAR instrument with the SAXS configuration, indicated by the long tube, i.e. a long sample to detector distance. To the right in the picture one can find the sample chamber. The detector is shown to the left.

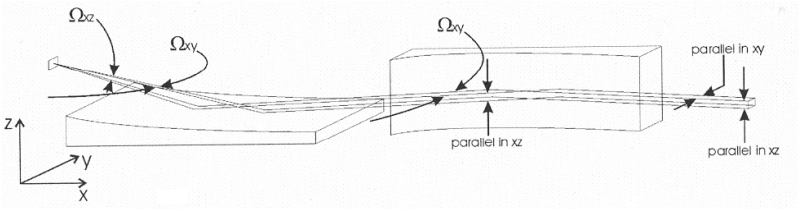

Figure 6.15: The Göbel mirrors. [30]

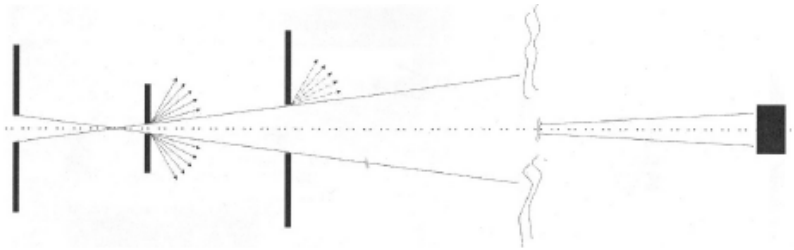

Figure 6.16: The pinhole collimating system principle. The first two pinholes limit the divergence whereas the third pinhole shadows the edge scattering of the second pinhole. [30]

The sample chamber has a software operated goniometer drive allowing for positioning of the sample in an xy-plane perpendicular to the incoming beam. This allows sample positioning over distances of 100 mm in y-direction and 80 mm in x-direction.

The HiStar detector is a two dimensional multiwire grid detector with pressurized Xe-gas which yields the opportunity to determine the x-positions and y-positions of X-rays in its imaging area. Noble gas atoms are ionized by incident X-rays, and these charged particles are attracted to and interact with electrodes to produce electrical signals indicative of the x-positions and y-positions of the original X-ray. [30]

Chapter 7

Chemical Compounds

7.1 Clays

Clays have played an important role throughout history and were among the first materials utilized by humans, as building materials and pottery. Nowadays clays have a vast range of applications in e.g. the oil and paper industry. [31, 32] The definition of clays was given in the nineteenth century based on their particle size, where particles with extension less than 2 μm were called clays. This was the limit of the optical microscope resolution, meaning that mineral particle beyond this limit were called clays. Although this definition no longer is sufficient, most particles of this size belong to the same mineral group and have a lot in common [18]. Clay as an object of scientific study was established in the 1930s. However, applications of clays beyond the traditional approaches are only in its infancy. Clays are now starting to be included together with other complex adaptive materials such as polymers, biomaterials and liquid crystals. [31, 33] Clays have been described as the materials of the 21st century. [32]

The clay minerals belong to the mineral group phyllosilicates. They can take a large variety of forms like amorphous, chain and layered structures, with primary plate let-shaped particles. Each of the platelets has a thickness of approximately 1 nm and a lateral size varying from tenths of nm up to a few μm. The structure of a single clay platelet is made up of tetrahedral and octahedral sheets in three dimensions. The ratio of each of these sheets divides the different clays into the 1:1 minerals and the 2:1 minerals, where the laponite RD and Ni-Fluorohectorite (NiFH) used in the current experiments belongs to the latter. [11, 34] The difference between 1:1 and 2:1 minerals are illustrated in Figure 7.1.

The 2:1 layer structure consists of one octahedral sheet sandwiched between two tetrahedral sheets. The 2:1 clay minerals are characterized by six octahedral sites and eight tetrahedral sites which forms the unit cell. When all six octa-

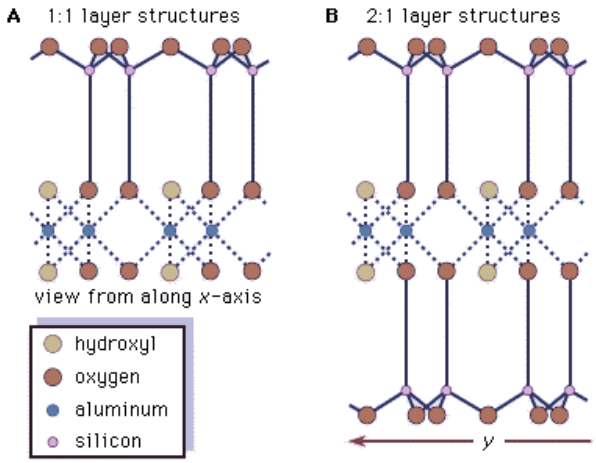

Figure 7.1: Schematic presentation of (A) 1:1 layer structures and (B) 2:1 layer structures. [35]

hedral sites are occupied, the structure is known as trioctahedral. When only four of the sites are occupied, it is refered to as dioctahedral. This is illustrated in Figure 7.2. The chemical formula is often reported on the basis of the half unit cell content, i.e., it is based on three octahedral sites. [32]

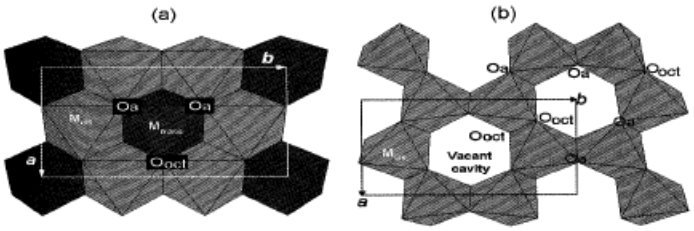

Figure 7.2: (a) Trioctahedral sheet, (b) Dioctahedral sheet. O_a represent the apical oxygen atoms shared with tetrahedra. O_{oct} is the anionic site shared between adjacent octahedra. [32]

The negative surface charge on the platelets causes them to stack with charge balancing cations such as Na^+ or K^+ in the interlayer. The longitudinal distance between two clay platelets is known as the basal spacing d_{001}, a characteristic property of each clay mineral. [11, 18] The edges of the platelets contains small amounts of pH-dependent positive charge and the magnitude of this charge divides the clays into groups. The members of each group are distiguished by the type and location of cations in the tetrahedral and octahedral sheets. [11]

7.1.1 Smectites

One of the subgroups of the 2:1 layered silicates is known as the smectites. These are among the most studied clays due to the vast range of utilizations. The laponite RD and the NiFH, used in the current experiments, are both members of this group. The charge density for smectites is relatively moderate, in the interval 0.4 - 1.2 $\frac{e}{unitcell}$. [11, 32] This moderate charge density allows penetration of water or other polar molecules which causes swelling, and also exchange of the interlayered cations. Figure 7.3 shows the structure of a smectite clay.

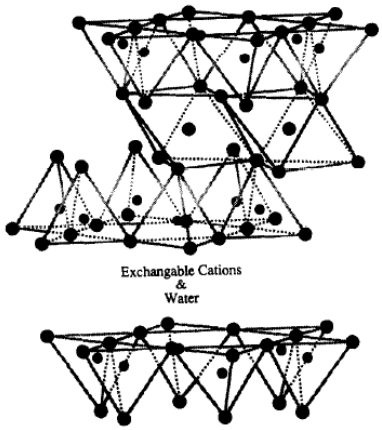

Figure 7.3: The structure of a smectic clay. [34]

Hectorite

Hectorite is a natural smectite clay mineral from altered volcanic tuff ash with a high silica content related to hot spring activity. Its name comes from the only place were the clay is mined viz. Hector, California. [36] The chemical formula is $Na_{0.3}(Mg, Li)_3Si_4O_{10}OH_2$ per half unit cell.

Ni-Fluorohectorite

Na-fluorohectorite (NaFH) is a synthetic chemistry customized clay mineral where the hydroxyls of normal hectorites have been exchanged with fluorine ions. NaFH has a large surface charge of $1.2\frac{e}{unitcell}$ (compared to the surface charge of laponite RD). It also has a large particle size, up to about 20000 Å in diameter. [37] This clay was purchased from Corning Inc. in powder form. The clay has the chemical formula $Na_{0.6}(Mg_{2.4}Li_{0.6})Si_4O_{10}F_2$ per half unit cell, where Na is an interlayer exchangeable cation. To create Nickel-Fluorohectorite

(NiFH), the NaFH clay was treated with an ion exchange method, where the Na^{+}-ions where exchanged with Ni^{2+}-ions. [11]

Laponite RD

Laponite is a synthetic layered smectite purchased from Rockwood as a powder. It has the chemical formula $Na^{+0.7}[Si_8Mg_{5,5}Li_{0,3}O_{20}(OH)_4]^{-0,7}$ and a surface charge of $0.4\frac{e}{\text{unitcell}}$. The structure is shown in Figure 7.4. Here, there are six octahedral magnesium ions between the two layers of four tetrahedral silicon atoms. These groups are balanced by twenty oxygen atoms and four hydroxyl groups. In a laponite crystal these unit cells are repeated in two directions, resulting in the disc-shaped particle shown in Figure 7.5 (a). With a thickness of only 1 nm, the platelets may be individually thought of as single crystals. [31] It has been estimated that a typicaly laponite crystal contains 30000 - 40000 unit cells. [38]

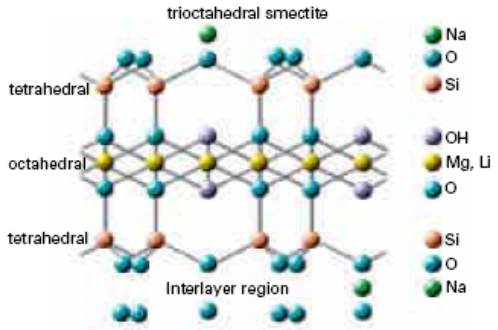

Figure 7.4: Schematic of a laponite particle. [38]

The negatively charged clay particles are neutralised with sodium ions absorbed on the surface, shown in Figure 7.4. Dispersed in water, the crystals are held together in stacks by a combination of electrostatic and osmotic forces, caused by these sodium ions in the interlayer regions, shown in Figure 7.5 (b). By adding polar compounds, e.g. a surfactant, the sodium can be held away from the particle surfaces, and allow cationic exchange [38]. A cationic exchange method is utilized in some of the experiments, further described in section 3.3, 7.3 and 8.3.

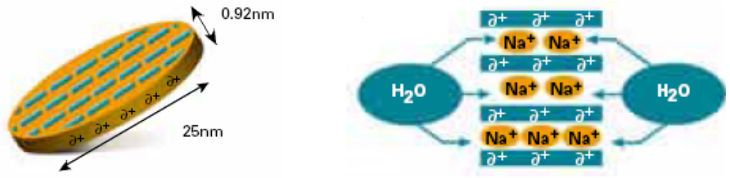

(a) (b)

Figure 7.5: (a): A laponite crystal, showing the dimensions and shape, (b): Schematic of laponite particles dispersed in water.

Alkyl Quaternary Ammonium Smectite

Alkyl Quaternary Ammonium Smectite (AQAS) is a surface modified laponite clay, see section 3.2. It is fabrically made lipophilic, which should ease the dispersion in the organic compounds utilized, viz. silicone oil and paraffin. This clay is a product sample from Rockwood.

7.2 Paraffin

Paraffins (alkanes) is a generic common name for a large number of homologous hydrocarbons which all have the same general chemical formula on the form C_nH_{2n+2}. These have successively higher density and boiling points with increased size, where the first four exist as gases in room temperature (25 °C), and the subsequently paraffins as liquids. When the paraffins contains $\sim$ 25 carbon atoms, they become solids. The paraffin wax used has approximately that number of carbon atoms. These waxes are white and partly transparent, as shown in Figure 7.6. The waxes have melting points in the range 44 °C−58 °C, and density in the range 0.88 $\frac{g}{cm^3}$ to 0.92 $\frac{g}{cm^3}$ [39].

Figure 7.6: Paraffin wax.

The wax consists of between 80 % and 90 % straight hydrocarbon chains. The balance consists of isoparaffins and cycloparaffins, shown in Figure 7.7.

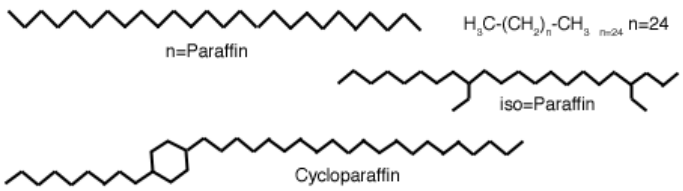

Figure 7.7: Drawing of paraffin wax molecules. [40]

Some other general properties of paraffin waxes are [40]:

- Non-toxic.
- Combustible.
- Non-reactive.
- Soluble in ether, benzene, and certain esters.
- Good water barrier.
- Extremely good electrical insulator, with surface resistivity ($\rho \approx 10^{15}\,\Omega$m) [41].

The paraffin wax used in the current experiments is shown in Figure 7.6. This wax has a melting point in the range $46\,^{\circ}$C$-48\,^{\circ}$C. It consist of a small amount of impurity sulphate (SO_4) $\leq 0.015\,\%$.

7.3 CTAB

CTAB - CethylTrimethylAmmoniumBromide has the chemical formula $C_{19}H_{42}BrN$, and is shown in Figure 7.8. It exists as a white solid powder in room temperature. It is a cationic surfactant, and is used to treat the laponite RD to make the clay particles lipophilic (see section 3.3) making it more soluble in paraffin and oil. The CTAB datasheet says that CTAB itself is solvable in ethanol and acetone. When the term CTAB is used in the description of the experiments it refers to the CTAB modified clay and not the CTAB itself.

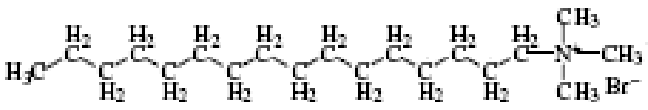

Figure 7.8: Schematic of the CTAB-molecule. [42]

7.4 Silicone Oil

The silicone oil used in some experiments was Dow Corning 200, 100 cS fluid, purchased from VWR. The silicone oil is analogous to the carbon based oil, with alternating silicone and oxygen atoms instead of the carbon atoms. The oil has a specific particle density of 0.973, slightly higher than the density of the paraffin wax. The conductivity is rather small, $\sigma_f(0) = 5.0 \cdot 10^{-12} \frac{\mathrm{S}}{\mathrm{m}}$ [43]. Unlike carbon-based oil, silicone oil is not flammable.

Part III

Experiments

Chapter 8

Clay Sample Preparation

8.1 Paraffin Samples

The samples consist of paraffin and clay, and as mentioned in the introduction three different kinds of clay species were investigated, viz. Laponite RD, AQAS, and CTAB-modified Laponite RD. The sample preparation was basically the same for all three kinds of clays. It can be summarized as:

1. Prepare the proper amount of paraffin in a container.
2. Melt the paraffin.
3. Prepare the proper amount of clay and mix it with the liquid paraffin, shaking the container.
4. Pour the dispersed clay onto the preheated cell. (See Figure 9.1 for the experimental setup)
5. Turn on the voltage and the heat off.
6. Let the paraffin solidify, turn off the voltage and cut out the sample.

The concentration of clay used was either $\frac{1\,\mathrm{g}}{10\,\mathrm{ml}}\frac{\mathrm{clay}}{\mathrm{paraffin}}$ or $\frac{2\,\mathrm{g}}{10\,\mathrm{ml}}\frac{\mathrm{clay}}{\mathrm{paraffin}}$. The exact mass density of the paraffin was unknown. A couple of tests were performed and the results gave values at the lower edge of the interval given in section 7.2. The tests suffered from considerable uncertainty due to losses, so the mass density was assumed to be slightly higher, $0.9\,\frac{\mathrm{g}}{\mathrm{ml}}$.[1] Due to fast sedimentation the actual concentration of clay in the finished samples was quite unstable and varied from sample to sample because the concentration depended on which height of the container the sample was taken from. However, the mass density errors were not important in the experiments.

[1] This corresponds to the tabulated value found in [41].

8.2 Silicone Oil Samples

The oil and clay samples were made easily by mixing the chosen concentration of clay into the silicone oil with subsequent shaking.

8.3 Surface modification of Laponite using CTAB

The properties of CTAB is described in section 7.3 and 3.3. The goal was to make the laponite lipophilic using CTAB. The procedure to do this was based on an article by Leach and Hopkinson et al. [44], where an analogous experiment was performed using DODAB[2] instead of CTAB. Our experiment was therefore slightly adjusted to fit the use of CTAB. All amounts of materials were half of the amounts used by Leach and Hopkinson et al. [44]. The following procedure was used:

1. Mix the proper amount (400 ml) of distilled water and CTAB (2.5 g) while stirring.
2. Heat to 80 °C and add the proper amount of ethanol (100 ml 20 %) while stirring.
3. Add the stoichiometric amount of laponite (7.53 g) while stirring.
4. Cool the solution overnight, covered and under stirring.
5. Filtrate the solution using 0.2 μm filter.
6. Stir the filtrated clay in a 125 ml half and half distilled water and ethanol solution.
7. Repeat this process (four times).
8. Dry overnight, heated to 100 °C.
9. Pulverize the clay with pestle and mortar.
10. Heat the clay to 100 °C for one hour.
11. Collect the finished clay in an airtight container.

8.3.1 Calculations

The calculations of the stoichiometric amount of clay were carried out based on the decision to use 2.5 g of CTAB.

[2] **D**imethyl di**o**cta**d**ecyl**a**mmonium **b**romide

The cationic exchange capacity (CEC) for laponite is[3] [34] 47 $\frac{\text{meq}}{100\text{g}} = 47\ \frac{0.001\,\text{mol}}{100\,\text{g}}$. In this experiment we decided to use an amount of CTAB corresponding to twice the CEC of laponite [45]. With a molar mass (Mm) of CTAB of 349.39 $\frac{\text{g}}{\text{mol}}$, we get the following calculations for the stoichiometric amount of CTAB needed per gram laponite:

$$\begin{aligned} 2 \times \text{CEC} &= 94\ \frac{0.001\ \text{mol}_{\text{CTAB}}}{100\ \text{g}_{\text{Lp}}} = \frac{0.094\ \text{mol}_{\text{CTAB}}}{100\ \text{g}_{\text{Lp}}} \cdot 349.39\ \frac{\text{g}_{\text{CTAB}}}{\text{mol}} \\ &= \frac{32.843\ \text{g}_{\text{CTAB}}}{100\ \text{g}_{\text{Lp}}} = 0.3284 \frac{\text{g CTAB}}{\text{g Laponite}}, \end{aligned} \tag{8.1}$$

where the relation $\text{M}_\text{m} = \frac{\text{m}}{\text{n}}$ was used in the calculation.

[3] This value is very uncertain. Different literature gives different values of the CEC, varying from 47-80 $\frac{\text{meq}}{100\text{g}}$ [34, 44, 45]. After some discussion it was decided to use the value 47 $\frac{\text{meq}}{100\text{g}}$. As shown by Velde [18], the CEC should be measured at neutral pH, since the surface cation concentration is pH-dependent. This fact may explain the variations in reported CEC-values.

Chapter 9

The Setup

The experimental setup is shown in Figure 9.1. The individual equipment devices used are described in detail in chapter 6. The cell is connected to the high voltage power-supply with $V_{in} = 6$ V, which gives $V_{out} = 2$ kV and $E_0 = 2\,\frac{kV}{mm}$, a well suited magnitude for ER performance. A voltage divider and multimeter is connected to the cell, controlling the voltage over the cell.

Figure 9.2 shows a close up of the cell while in use. One can clearly see the clay chain formation between the electrodes. The paraffin is still liquid though, and the chains are not always that easy to visually observe when the paraffin solidify. Figure 13.4 in chapter 13.1 is a picture taken of the same sample as in Figure 9.2 below.

In some experiments the cell was placed directly on the glass surface, as in Figure 9.2. The paraffin sticks very easily to glass and problems often occurred with removing the cell and the sample without destroying one or both of them. In some of the experiments, a plastic film, called polyimide, was put between the glass surface and the cell to avoid this, shown in Figure 9.1 (b), which proved to be an excellent material for the purpose. This was a suitable approach when the sample had to be removed for observation with e.g. AFM or SAXS. For observation in light microscope, the sample was much easier to observe when it was still on the glass plate, which means that the cell was removed, not the sample, avoiding the sample to twist or deform.

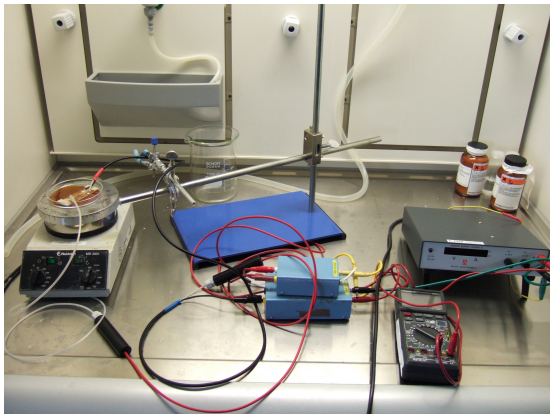

(a)

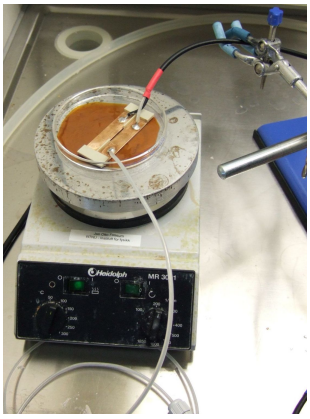

(b)

Figure 9.1: (a): The experimental setup, (b): Close view of the cell.

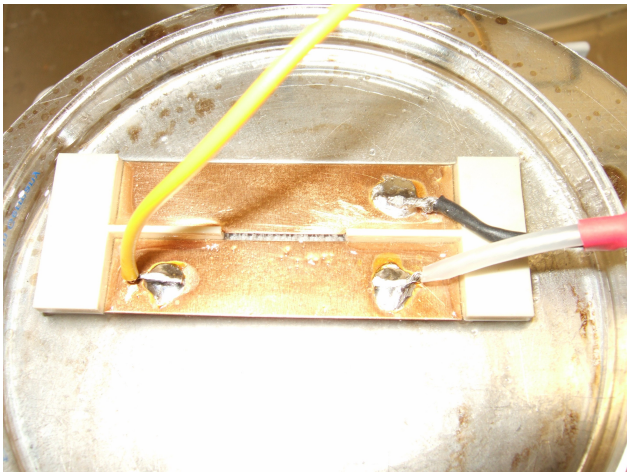

Figure 9.2: Chains of CTAB-treated laponite in liquid paraffin under the application of 2 kV.

Chapter 10

X-ray Scattering

X-ray scattering experiments were performed using the equipment, described in section 6.12. The objective of the experiments were to detect the existence of electrorheological effect, i.e. chain formation visible as anisotropic scattering data in the paraffin and clay samples, and to examine differences between the clay species, both with SAXS and WAXS. In the case of the silicone oil experiments the objective was to investigate the dynamics of the ER behaviour. There were performed three different kinds of scattering experiments. Two with paraffin samples, SAXS and WAXS, and one SAXS on oil samples.

Fourteen different paraffin samples were investigated, the ten first of them were placed in the same sample holder and scanned both with SAXS and WAXS. They were:

- Pure paraffin, as a reference.
- Dispersion of AQAS without applied field, as a reference.
- Two samples of AQAS with different orientation.
- Dispersion of Laponite RD without applied field, as a reference.
- Two samples of Laponite RD with different orientation.
- Dispersion of CTAB without applied field, as a reference.
- Two samples of CTAB with different orientation.

The different orientation of the samples are showed in Figure 10.1. One sample was scattered from above, Figure 10.1 (a), and one from the side, Figure 10.1 (b).

In addition to the first ten paraffin samples, three different samples with Nickel-Fluorohectorite (NiFH) were investigated with SAXS scans. The first without any applied field. The difference between the other two NiFH samples (with

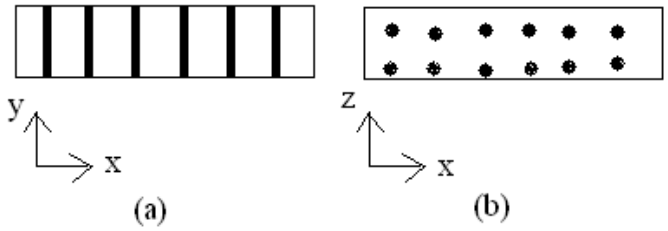

Figure 10.1: Different orientation between the samples with the same clay species. One sample, (a) was scattered from above, the width of the chains, and one (b) was scattered from the side, the heigth of the chains.

applied field) were the clay concentration. These samples are referred to as NiFH high and NiFH low. The last paraffin sample was an AQAS sample with high clay concentration, refered to as AQAS high.

The oil experiments were performed using AQAS and NiFH. An electrorheological cell was filled with the oil suspension and the electric field was applied. The cell consisted of two Cu-electrodes with a 2 mm gap between them. The electrodes were coated with a kapton film, an X-ray transparent material, to keep the oil suspension from floating away. The field strength was 1 $\frac{\text{kV}}{\text{mm}}$ in all the oil experiments. A closer description of the cell can be found with Parmar [11].

Before the scattering scans could be performed, initial nanography scans were carried out to localize the sample positions. Nanography scans shows different colours for different intensities and it is hence easy to determine the different positions of the samples, the sample holder and the sample chamber. These nanography scans were not always optimal to find the exact positions, so some of the samples had to be scanned at different positions to hit correctly. Several scans at different positions were often required to detect an area where ER behaviour was present.

10.1 WAXS

All the WAXS scans had a sample-detector distance of 26 cm, and the counting time was 120 s. In addition to the ten clay samples described, an empty cell scan was performed to invesigate the strength of the background scattering. WAXS scans should give information of the particle orientation, i.e. the microstructure of the clay.

10.2 SAXS

All the SAXS scans had a sample-detector distance of 106 cm. The counting time was different for different samples, varying between 120 and 2400 seconds. A typical scan started at $240 - 300$ s, and was rescanned with higher counting time if the sample proved interesting. SAXS scans should give information of the macrostructure of the clay chains.

Chapter 11

Atomic Force Microscope

All the AFM-experiments were performed in tapping mode, and the equipment used is described in section 6.11. The experiments are done in collaboration with Dr. Ahmed Gmira.

The investigated clay was AQAS. Three different samples were scanned, one pure paraffin and one suspension of AQAS and paraffin without field influence, both for comparison, and finally the AQAS sample with ER chains present.

Chapter 12

Sedimentation Tests

One of the major problems of making effective ER fluids, and hence ER devices, is the sedimentation which often, at least in some of the current paraffin experiments, can be so fast that measurments are diffucult due to a too low particle concentration in the fluid. To try to reduce the total sedimentation and increase the sedimentation time, different approaches were used. The two major factors that could be altered were the liquid temperature and the particle size. The surface cationic exchange modification comes in addition. The particle size was altered by the ultrasonic bath, which, to some extent, dissolves large aggregates and flocculations.

12.1 Sedimentation in Laponite RD

These experiments were performed using three equivalent containers of the same amount of a Laponite and paraffin suspension. The temperature were increased in discrete steps of 10 °C, from 70 - 120 °C, where visual sedimentation time data were collected at each step. The results of these tests are shown in section 14.1. Some sedimentation tests with paraffin and Laponite RD were also carried out with the rheometer, shown in section 17.3.

12.2 Sedimentation-alterations Using Ultrasound

12.2.1 Visual Sedimentation Tests

Paraffin samples containg AQAS were melted in advance and a visual sedimentation test was performed. A mark was set at the height of the sediment. The sample was then dispersed by shaking and placed in the ultrasonic cleaner at

approximately 55 °C and exposed for 90 min. A new sedimentation test was then performed and a new mark was set. The sample was then cooled to solidification. Finally the sample was heated again and a new sedimentation test carried out, to check what effect solidification of the paraffin had on the clay particle distribution. Similar tests were performed using silicone oil as liquid, omitting the solidification part.

The AQAS clay was chosen in these experiments because the clay had shown the lowest and slowest sedimentation (compared to Laponite RD and CTAB). The results of these tests are shown in section 14.3.

12.2.2 Sedimentation Picture Series in Crossed Polarizers

To observe the sedimentation over a larger time scale, i.e. $\sim$ 24 hours, series of pictures taken in crossed polarizers were executed. These experiments were done in collaboration with Nils Ivar Ringdal with his experimental setup. The polarizers should be about 99 % effective, meaning that they transmit 99 % of the incident light in the intended polarization direction. The sample containers used, called vitrotubes, hold approximately 1 ml liquid. The width of the container is 1 cm and the depth is 1 mm, meaning that the pictures are almost two-dimensional.

Three different sample series were taken. One AQAS-series not exposed to ultrasound. The other two samples were both exposed, on different temperatures, 23 and 57 °C, to investigate possible temperature differences. Series of approximately 600 pictures were taken for all of the samples, with intervals of one or three minutes. Results of these experiments are shown in section 14 and on the enclosed DVD.

Part IV

Results & Analysis

Chapter 13

Light Microscopy

13.1 Paraffin Samples

Hardly any studies of frozen electrorheological structure have been published previously.[1] One published article has been found, written by Lan et al. [46] It describes ferroelectric triglycine sulfate ($(NH_3CH_2COOH)_3 \cdot H_2SO_4$) particles dispersed in an unspecified wax. The scientific focus in this article is quite different from the experiments described in this thesis, so any comparison would not be appropriate.

Figure 13.1 - 13.3 shows chain formation in laponite RD. The chains can be seen as columns across the sample. The gap in the cell is 1 mm, so all the pictures from 13.1 - 13.5 shows 1 mm broad samples. In Figure 13.1 (a) and in Figure 13.2 the uppermost paraffin surface of the sample was removed to access the laponite chains directly. Figure 13.3 show samples where the surface is intact, and they appear quite different visually. Figure 13.1 (a) shows a sample with pure paraffin. It is easy to see the difference between pure paraffin and the clay dispersions. The paraffin sample was created using exactly the same procedure as with the other samples, i.e. the same field strength was applied. All these pictures show broad chains or columns. This indicates a high electric field strength. (The thickness of the chains are further discussed in section 13.2.) The actual field strength was not measured exactly but should be approximately 2 $\frac{\mathrm{kV}}{\mathrm{mm}}$ (A cell without the possibility to measure the voltage was used, and the field strength was calculated from the power-supply display.)

Figure 13.4 shows chains of the CTAB modified clay. These chains appears quite different from the RD chains. They are bluish and irregular, although the colour is most likely created by the settings of the microscope and the software, and is not the natural colour, since no blue colour was visible under

[1] As least not according to an extensive litterature search on the topic.

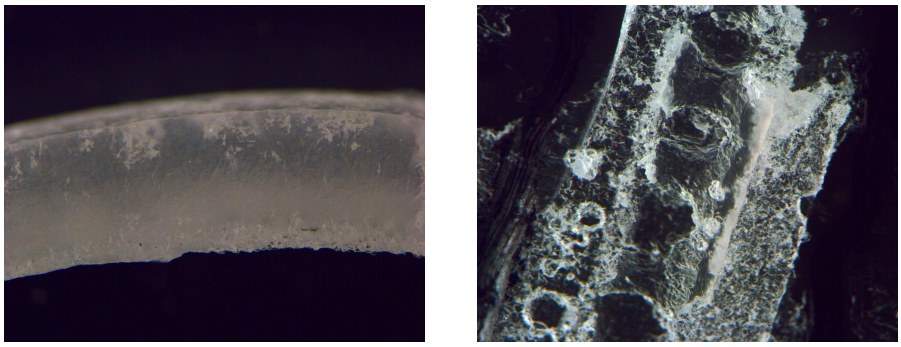

(a) (b)

Figure 13.1: (a) A sample of pure paraffin. (b)Laponite chains formed with 2 kV voltage applied. The cell gap and hence the chains are 1 mm across.

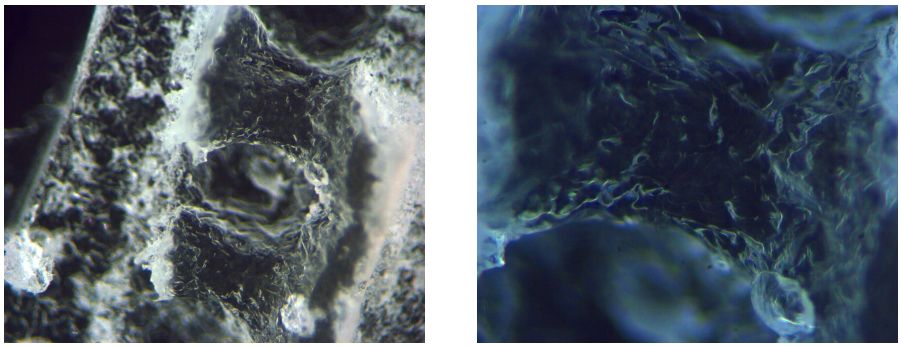

(a) (b)

Figure 13.2: (a) Laponite chains formed with 2 kV voltage applied. The cell gap and hence the chains are 1 mm across. (b) Closer view of a single chain.

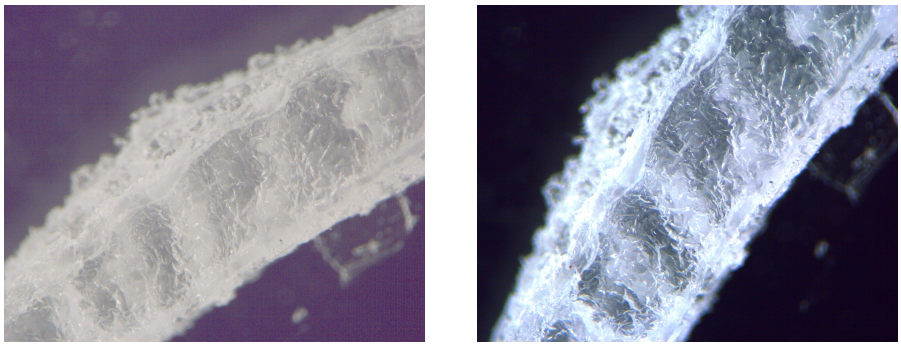

(a) (b)

Figure 13.3: Laponite chains formed with 2 kV voltage applied. The cell gap and hence the chains are 1 mm across.

the experiment (See Figure 9.2), and no other CTAB experiments showed the blue colour. Figure 13.5 shows chains of AQAS. These chains are more narrow and vague than for laponite RD. The difference between Figure 13.5 (a) and (b) is the production routine. In (a), the sample is sticked to a glass surface beneath the cell so that the sample is horizontal, and the chains are unaffected. In (b), the sample is cut out from the cell. The sample has twisted and are difficult to focus with the camera. There were difficulties for both the AQAS and the CTAB to get good pictures of the chains. Since these two clays are lipophilic, they disperse much better in paraffin and oil than Laponite RD. The chains are thus narrower than for Laponite RD, and ideally there could be chains of single particles, invisible to the light probe. In addition, the ER effect is expected to be weaker for AQAS and CTAB compared to RD due to the lower relative clay concentration.

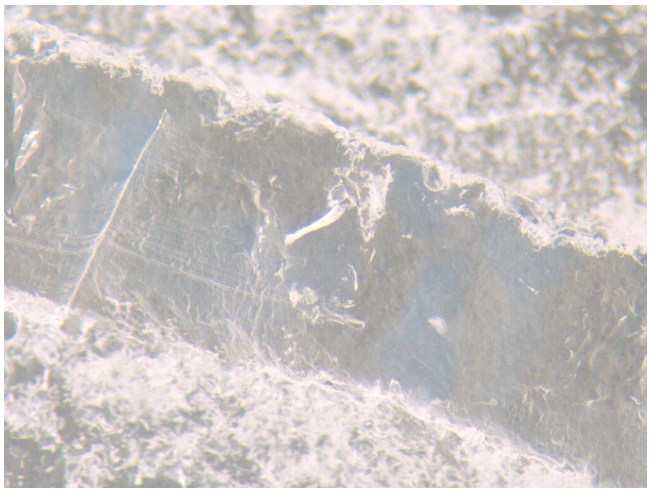

Figure 13.4: Chains of CTAB in paraffin. The cell gap and hence the chains are 1 mm across. The field strength is $2\frac{\mathrm{kV}}{\mathrm{mm}}$.

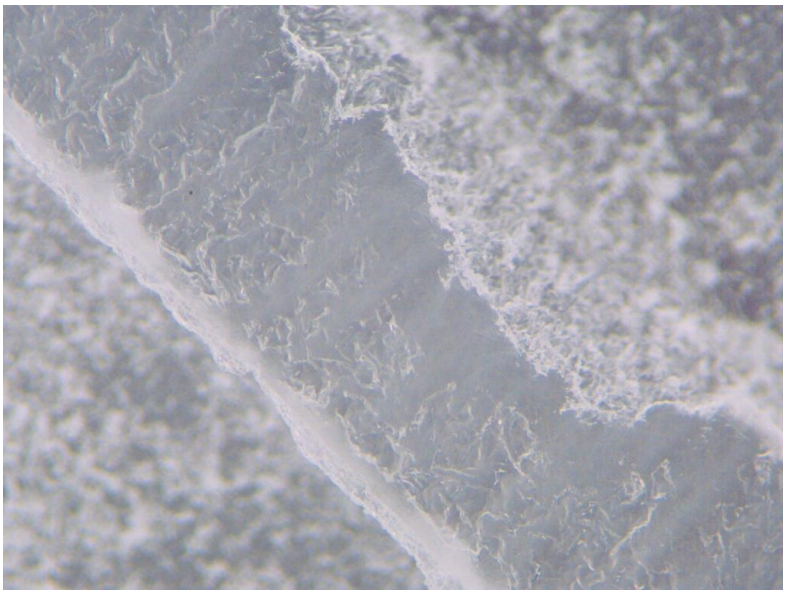

(a)

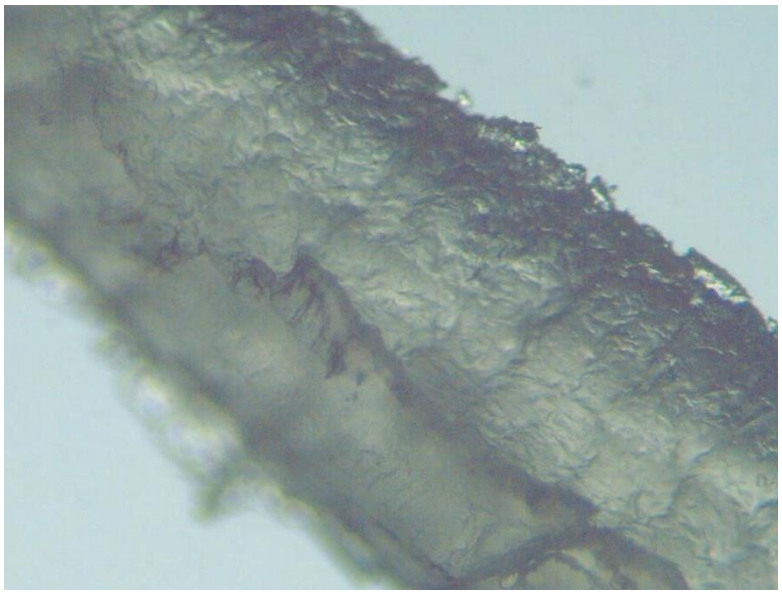

(b)

Figure 13.5: Chains of AQAS in paraffin. The cell gap and hence the chains are 1 mm across. The field strength is $2\frac{\mathrm{kV}}{\mathrm{mm}}$.

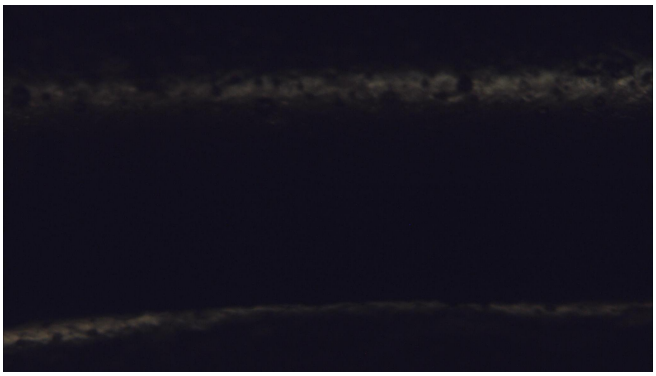

(a)

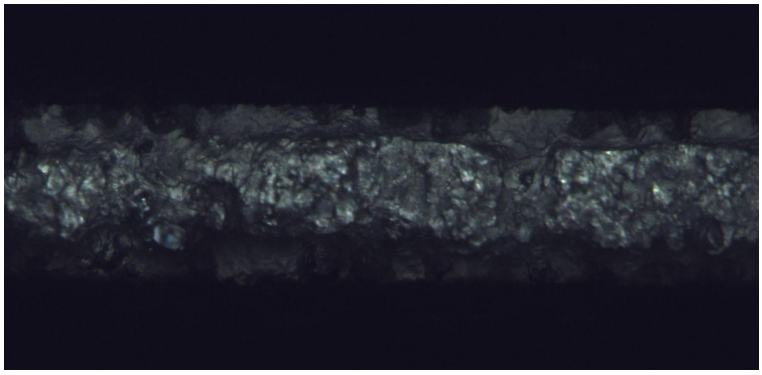

(b)

Figure 13.6: (a) Pure paraffin in crossed polarizers, (b) Chains of Laponite RD in crossed polarizers. The field strength is $2\frac{\text{kV}}{\text{mm}}$. The anisotropic nature of the picture indicates present ER effect. Both samples has a width of 1 mm.

Figure 13.6 shows two pictures taken between crossed polarizers. Figure 13.6 (a) is pure paraffin, and appears almost black as predicted from the theory (see chapter 5). Figure 13.6 (b) is a sample of paraffin and laponite RD. This sample is clearly visible which indicates anisotropic nature and thus present ER effect. The ER effect, i.e. the chain structure, can also be detected directly by visually investigation.

13.2 Oil Samples

Figure 13.8 shows the development of chains of laponite RD in silicone oil when an increasing external electric field is applied. It is apparent that the particles are gathering to form chains when the field strength is increasing, and subsequently to form colums of the chains. Observe especially the difference between Figure 13.8 (c) and (d). This corresponds well to the prediction of the creation of columns for high field strengths [6]. Figure 13.7 shows a closeup of a single column at $E = 1.5\ \frac{kV}{mm}$. It contains a very large quadratic particle, approximately 130 μm wide.

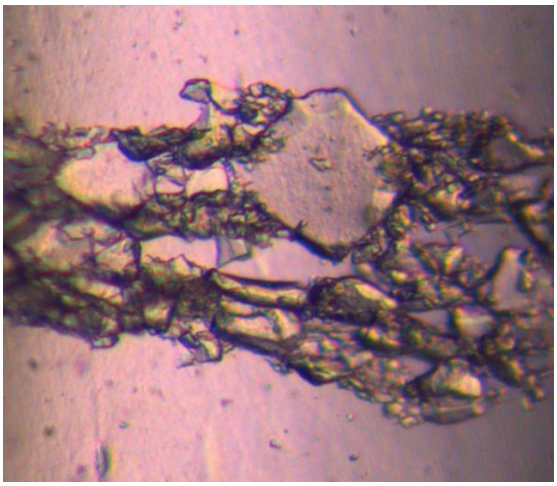

Figure 13.7: A single column of Laponite RD particles in silicone oil formed with a field strength of $1.5\frac{kV}{mm}$. The width of the picture is approximately 350 μm. The large particle is nearly quadratic with a size of approximately 130 μm along the edge.

13.3 Electrorheological Dynamics

Several films of the ER experiments were recorded. These films are recordings of clay dispersions in silicone oil only, since the heating could not be used with the microscope, hence precluding the use of paraffin. Some of the films are found in the "ER films" folder on the enclosed DVD. An index of the films, with explaination to each of them are to be found in Appendix A. These films illustrates the ER effect on the fluid flow, the creations of chains and further to the creation of columns, and separates the fluid above and below the threshold voltage.

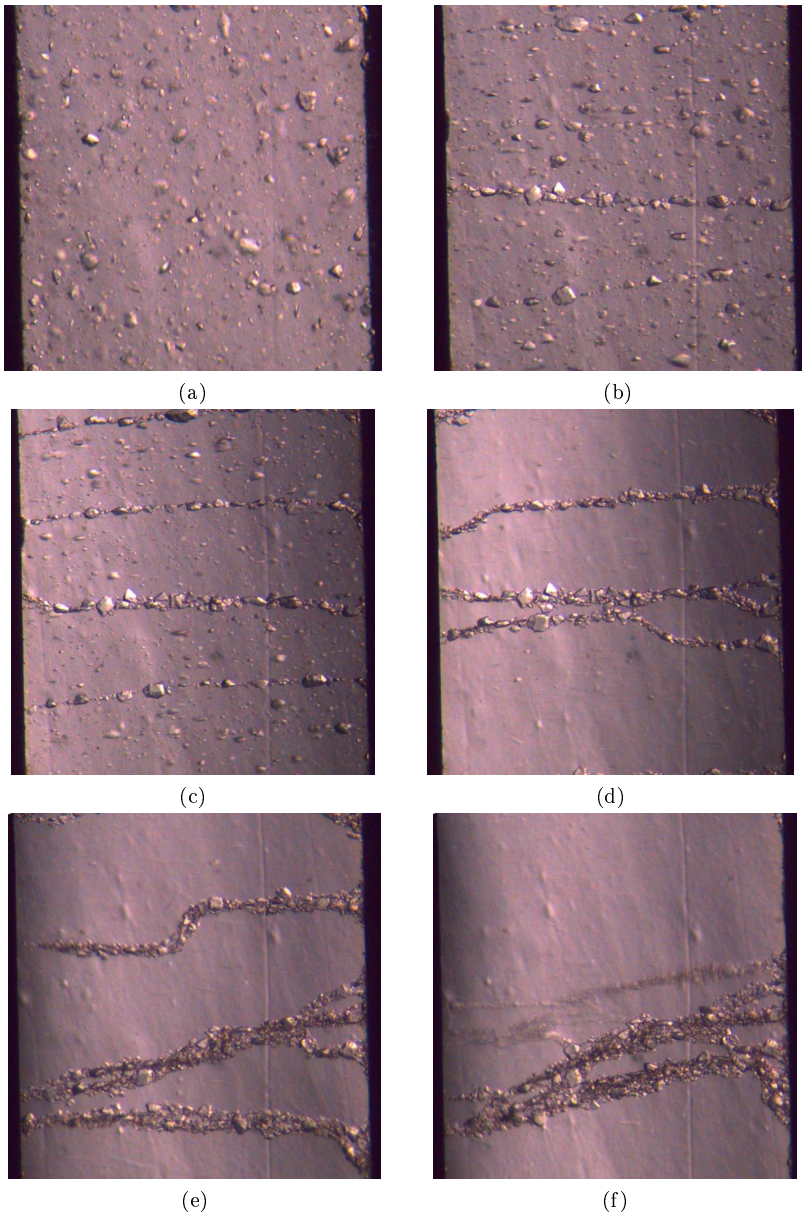

Figure 13.8: Showing the development of RD chains in silicone oil. (a) No applied volage E = $0\frac{\text{kV}}{\text{mm}}$, (b) E = $0.5\frac{\text{kV}}{\text{mm}}$, (c) E = $0.5\frac{\text{kV}}{\text{mm}}$ Picture taken a few seconds after (b), (d) The chains are starting to form columns E = $2\frac{\text{kV}}{\text{mm}}$, (e) E = $3\frac{\text{kV}}{\text{mm}}$, (f) E = $3\frac{\text{kV}}{\text{mm}}$ Picture taken a few seconds after (e). All pictures has a width of 1 mm.

13.4 Threshold Voltage

The threshold voltage was measured for the Laponite RD, AQAS and CTAB, dispersed in silicone oil. It gave the following results:

- $V_{T_{RD}} = 240$ V.
- $V_{T_{AQAS}} = 229$ V.
- $V_{T_{CTAB}} \approx 265$ V.

The voltages were measured under observation with light microscope. The cell was given a small gradient to give the dispersion a flux. When the flux stops, a phase transistion from liquid to solid is about to occur, an indication of present ER effect. The threshold voltage is a measure for the lowest voltage needed to start particle movement in the direction of, or parallel to, the electrical field, and not always the voltage for the creation of visible chains. Small particles will require less field strength than large to arrange themselves, and chains invisible to the microscope can be created before any observable chains are detected. The CTAB clay did not have a homogenous (compared to the other two clays) particle size distribution, and was probably the reason why the threshold voltage varied to some extent. Figure 13.9 shows the chain formation of CTAB at the threshold voltage, in this case 270 V. The large difference in particle size is evident. Any threshold voltage measurement for clay in paraffin could not be performed, since any arrangement with heating on the microscope was difficult. However, it is reasonable to expect the threshold voltage to depend on the viscosity of the liquid, i.e. low V_T for low η and vice versa. Usually, the operation field strength for ER performance is in the order of 1 $\frac{\text{kV}}{\text{mm}}$ [2,10]. However, studies on the ER effect on voltages as low as 0.33 kV has been done by Powell [47]. This ER fluid with the exact same carrier liquid, the silicone oil, but with starch particles instead of clay, showed newtonian behaviour at 0.33 kV and non-newtonian at 0.66 kV. Since the behaviour of the ER fluid is dependent of (the unknown) particle size and the permittivity ϵ_p of the particles, according to equation 2.1, any immidiate comparisons can not be made at this point.

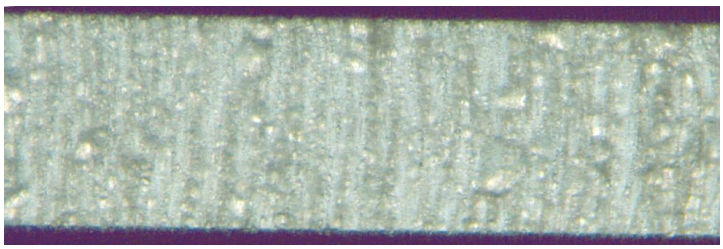

Figure 13.9: Showing chains of CTAB at the threshold voltage (270 V). The chains are 1 mm long.

Different experiments performed immediately after each other, with the same sample at the same voltage, could show different behaviour. Although the threshold voltage would be the same, one experiment could yield visible chains at the threshold while the other could require voltages up to 1.5 kV to detect any. A reasonable explaination for this could not currently be found. This phenomenon can be seen in film V1 on the enclosed DVD. A description of the film can be found in Appendix A.

Chapter 14

Sedimentation Tests

Remark: The volume fractions Φ used for AQAS and CTAB were always calculated using the density of laponite RD. This is erroneous, and the given values for the volume fraction in chapter 14 and chapter 17 should be considered somewhat lower. The density of AQAS and CTAB should be approximately identical.

14.1 Sedimentation of Laponite RD in Paraffin

One of the greatest challenges for applications of ER fluids, is the problem with particle sedimentation (See chapter 2.2). The sedimentation time, i.e. the time it takes for the particles in a sample to settle, decreases with increased temperature, as shown in Figure 14.4, and since the paraffin has its melting point at around 50 °C, fast sedimentation is expected to occur. In reality, the paraffin temperature used in the experiments was higher than 50 °C, to be able to work with the liquid paraffin in room temperature, and consequently the sedimentation problem increased as well. Figure 14.1 shows two paraffin samples, both at a temperature of approximately 80 °C. The right sample is already completely sedimented for comparison. The pictures are taken at 0 s, 8 s and 30 s. The clay concentration in the upper part of the fluid is too low to be used in ER experiments after a few seconds. This problem was a challenge, especially in rheometer experiments where the sample is at rest for some time before the measurement starts. This is illustrated in Figure 14.2. The data at 70 and 80 °C is clearly measured on already sedimented samples. Figure 14.2 also shows the temperature dependence on the viscosity.

In oil, the time it takes to sediment the laponite RD is approximately 30 minutes at room temperature (25 °C). A complete sedimentation takes several hours. This difference could be explained by the large difference in viscosity. Figure 14.3 shows the sedimentation of laponite RD in silicone oil for different volume

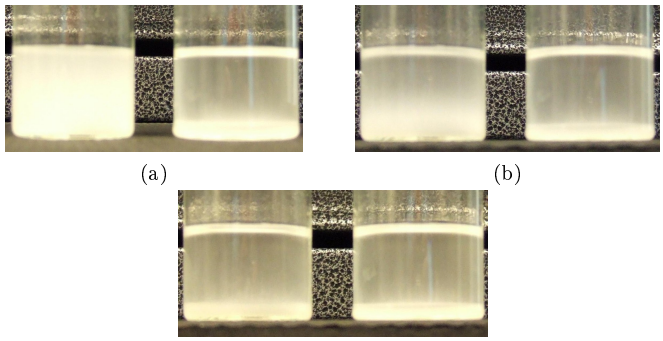

(a) (b)

(c)

Figure 14.1: The pictures in (a) to (c) show the sedimentation of Laponite RD in paraffin at t = 0, 8 and 30 s, respectively. The right sample in all pictures is completely sedimented.

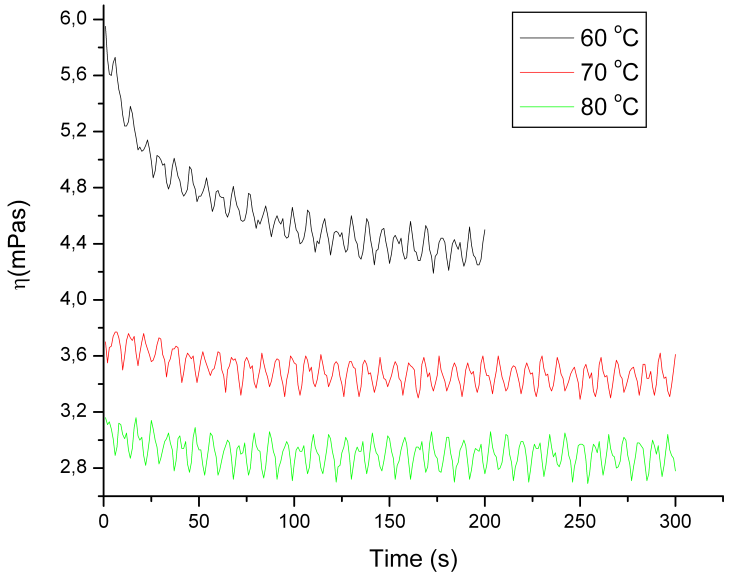

Figure 14.2: Sedimentation time for Laponite RD in paraffin at three different temperatures, 60, 70 and 80 °C. The sedimentation was so fast for the two highest temperatures that the dispersion was completely sedimented before the measurment could be started. Sheared with a constant shear rate $\dot{\gamma} = 10\frac{1}{\mathrm{s}}$

fractions at 25 °C. This shows a completely different behaviour than the paraffin samples. Of course, the large difference in temperature plays a major role here.

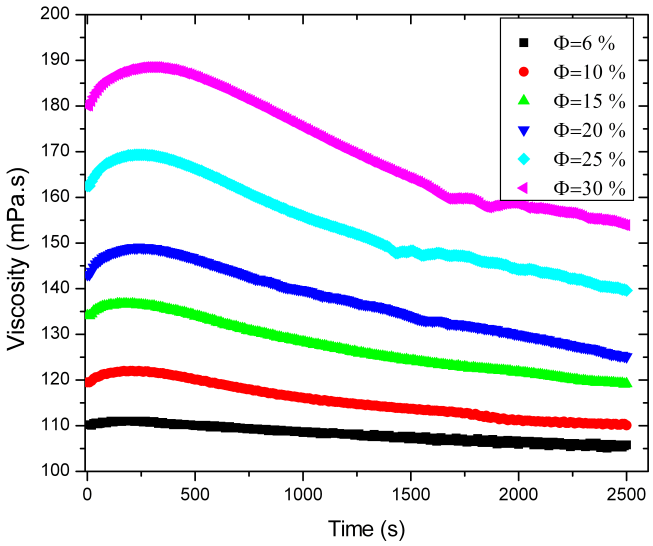

Figure 14.3: Sedimenation for Laponite RD in oil for different volume fractions. Sheared with a constant shear rate $\dot{\gamma} = 10\frac{1}{\mathrm{s}}$. Experiment performed by Børge Aune Schjelderupsen.

In Figure 14.4 the sedimentation time was plotted as a function of temperature. Clearly, the sedimentation time decreases for increasing temperature, as predicted in the theory. An interesting feature though, is the fact that this relation neither seems to be exponential, as in equation 2.3, nor linear. At certain temperatures, between 80 and 90 °C, and between 100 and 110 °C, the decrease in the sedimentation time is slowed down, and in one case, in fact increasing. This increase was also present in other sets of experiments. The experiments did suffer from a large uncertainty though, since the time of sedimentation was determined visually and was thus discretional. Large intervals between measurments should also be taken in account. However, this characteristic behaviour was fully reproduceable, but an explanation of the phenomenon was not found. (A suggestion could be water effects near its evaporation temperature.) An investigation of the sedimentation could be an interesting topic for future study.

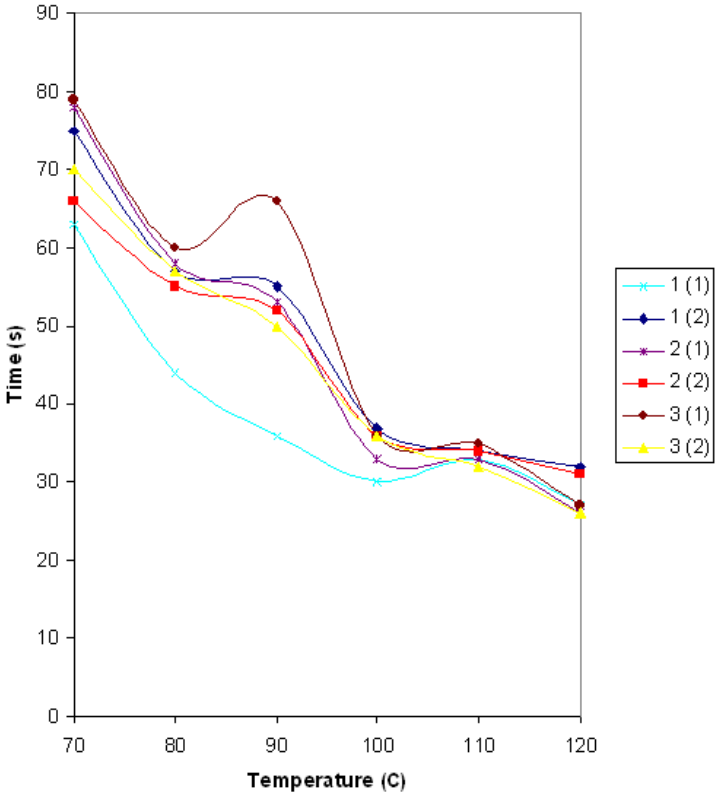

Figure 14.4: The sedimentation time for Laponite RD in paraffin at different temperatures. The number from 1-3 represent different but equally prepared samples. The numbers in parenthesis represent different series of measurment.

14.2 Sedimentation of Modified Clays in Paraffin and Oil

When trying to disperse the modified AQAS clay in paraffin, it was discovered that the sedimentation time was significantly slower than for the normal laponite RD, also at high temperatures (up to 130 °C). Some improvement was expected because of the solubility of AQAS in oil and paraffin. The sedimentation in CTAB modified clay was somewhere in between the AQAS and RD, indicating some effect of the ionic exchange. The CTAB clay contained a large amount of big particles due to insufficient crushing in the production of the clay, which could affect the sedimentation time.

14.2.1 AQAS

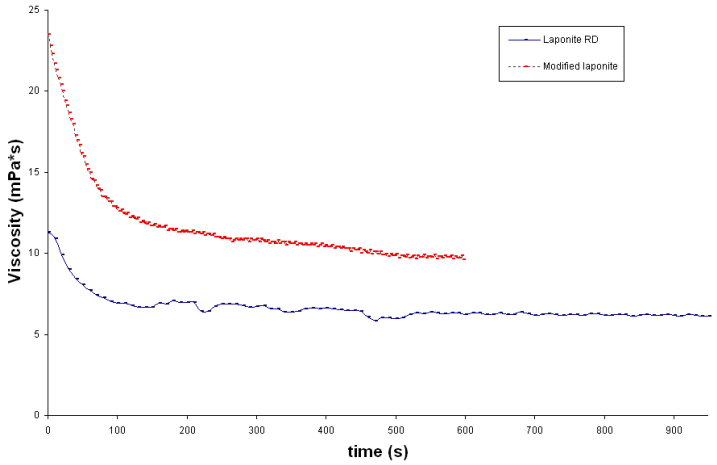

Figure 14.5: The sedimentation in samples of equal concentration of laponite RD and AQAS in paraffin. The RD experiment was performed at 50 °C, and the AQAS experiment at 52 °C. Sheared with a constant shear rate $\dot{\gamma} = 10\frac{1}{\mathrm{s}}$.

Figure 14.5 shows the difference between the sedimentation in laponite RD and AQAS in paraffin. The lipophilic AQAS is better dispersed in the paraffin than RD and thus sediments slower. Figure 14.6 shows the sedimenation for AQAS in oil at 60 and 70 °C. This shows that the viscosity is strongly temperature dependent for silicone oil. Comparing Figure 14.6 with 14.7, the different behaviour of the samples become evident. In Figure 14.7 (and also in Figure 14.3 for the RD samples), the viscosity has a characteristic initial increase in viscosity during shearing. This feature is apparently absent for high temperatures.

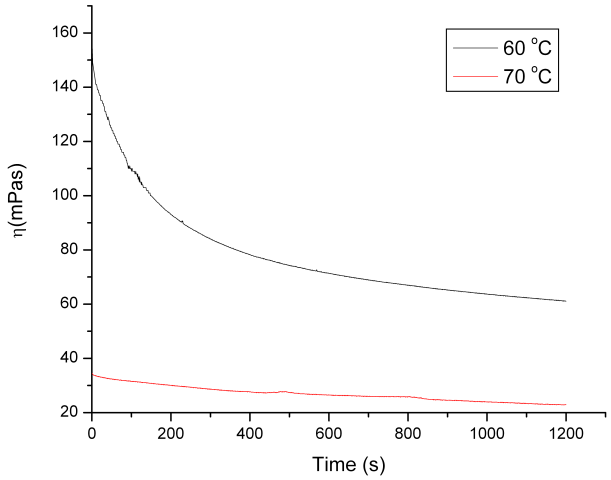

Figure 14.6: The sedimentation time for AQAS in oil at 60 °C and 70 °C. Sheared with a constant shear rate $\dot{\gamma} = 10\frac{1}{\text{s}}$.

14.2.2 CTAB

A sedimentation test was performed on the CTAB sample with volume fraction Φ=0.2, shearing the sample at a constant shear rate $\dot{\gamma} = 10\ \frac{1}{\text{s}}$ for 2500 s while observing the viscosity. The viscosity as a function of time is shown in Figure 14.8 for the CTAB modified laponite together with a laponite RD sample (Φ=0.15) and a AQAS sample (Φ=0.1).

The viscosity of the laponite RD sample decreases with over 10 mPa·s over the time periode. This is due to the sedimentation. The viscosity of the CTAB does not decrease very much with time, and this suggests that the sedimentation is much less than for laponite RD dispersions. This was also verified by visual sedimentation tests. The AQAS was also tested for comparison. For this sample the viscosity did not decrease during shearing, but rather increased a bit.

An interesting discovery, but not further investigated, was the properties of the sedimentation of CTAB in oil. Over long time periods, both for normal laponite RD and the AQAS, the sedimenation is complete, i.e. leaving two phases, the sediment phase and one fluid phase on the top with none or very few visible clay particles. With CTAB there are also two detectable phases, but the uppermost phase contains particles, most likely an isotropic phase, see Figure 14.9.

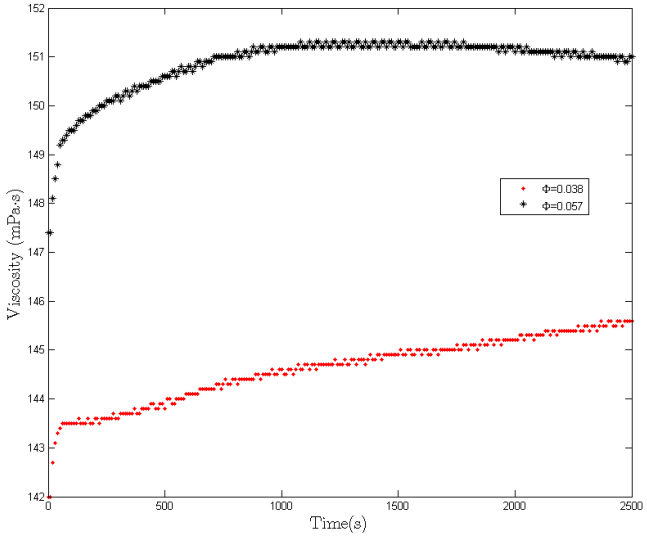

Figure 14.7: The sedimentation time for AQAS in oil at 25 °C for two different volume fractions. Sheared with a constant shear rate $\dot{\gamma} = 10\frac{1}{s}$. Experiment performed by Børge Aune Schjelderupsen.

14.3 The Effect of Ultrasound on the Sedimentation Rate

The sedimentation rate of AQAS in paraffin was tested before and after use in an ultrasonic cleaner (UC), see section 6.9. The ultrasound should cause the clay to disperse better. The samples were exposed for 90 min. Figure 14.10 (a) shows a sample after exposure to ultrasound, and after a complete sedimentation has settled. The blue mark indicates the pre-ultrasound sedimentation height. This shows that the UC has a formidable effect on the sedimentation rate. The sample was then brought to solidification with subsequent reheating, to investigate whether the solidification of the paraffin destroys the UC effect. Figure 14.10 (b) shows the same sample as in Figure 14.10 (a). The upper blue mark indicates the level of sedimentation after UC exposure. The middle bllue mark indicates the level of sedimentation after solidification and reheating, showing that the paraffin solidification attenuates the effect from the UC, but did not entirely destroy it. Similar tests, without the solidification-reheating, were performed with Laponite RD. These tests also showed a positive effect on the sedimentation rate.

A similar test, as described above, was performed on laponite RD in silicone oil. Figure 14.11 show the results of the experiment. The ultrasound causes the

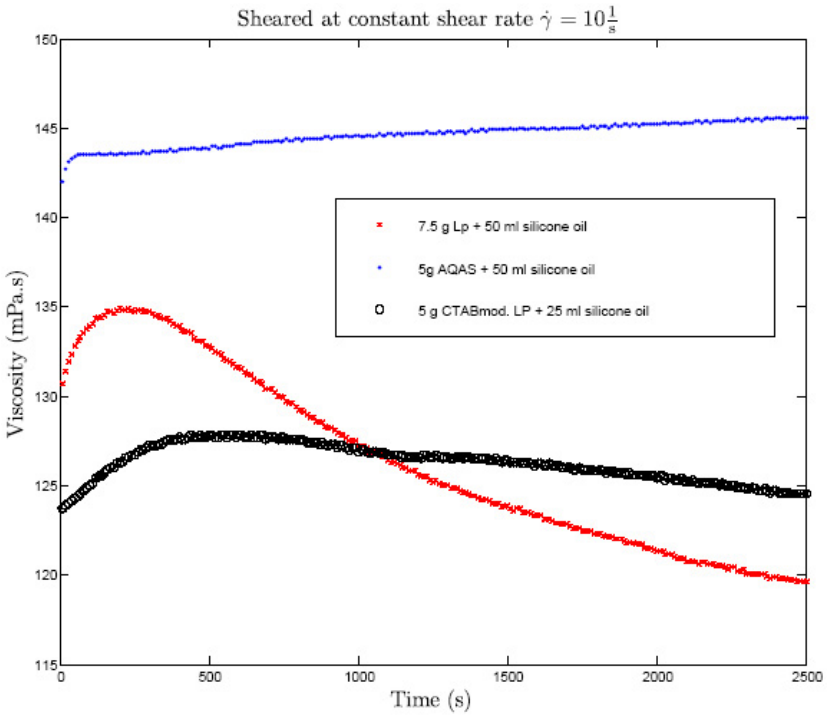

Figure 14.8: Viscosity vs. time at constant shear rate $\dot{\gamma}$=10 $\frac{1}{s}$ for a laponite RD, CTAB and AQAS

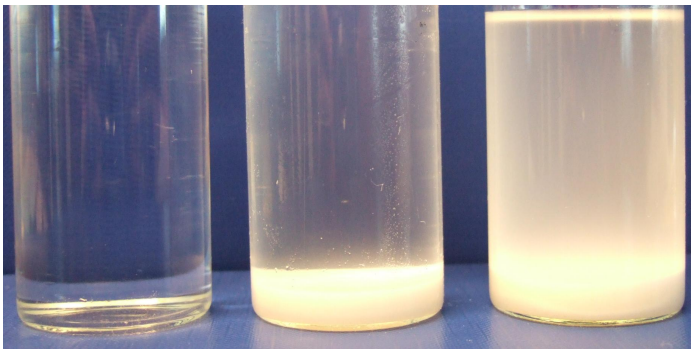

Figure 14.9: Pure silicone oil, laponite dispersed in oil and sedimentation of CTAB treated laponite dispersed in oil, from left to right.

sediment heigth to ascend somewhat. However, this seems to come from the fact that the upper phase contains less particles, not that the particles are better distributed in the liquid, which seems to be the case with paraffin samples.

The UC instrument has the opportunity to heat the samples up to 60 °C. The heating was used several times at different temperatures chosen more or less randomly. This gave a premonition for the UC effect to be stronger for low temperatures than for high temperatures. Series of sedimentation experiments with AQAS in silicone oil were performed, as described in section 12.2.2. Three films of the experiments were made, AQAS without UC exposure, AQAS with UC exposure at 23 °C and AQAS with UC exposure at 57 °C. These films can be found on the enclosed DVD as V6, V7 and V8. They should be watched simultaneously for a good comparison. A description of the films can be found in Appendix A. Figure 14.12 shows the first picture taken of the three different samples. The liquid height are slightly different in the three samples. The amount of clay likewise. Since only 1 ml liquid was used, even small differences would be visible. Figure 14.13 shows the last picture taken from each of the samples, after a complete sedimentation has taken place. The total sedimentation is clearly improved for both the samples with ultrasound exposure. The upper phase shows greater stability after ultrasound exposure. The high temperature sample seems to have achieved the best result, i.e. the highest sediment height, in contradiction of the expected result, but the error of different clay and oil amount makes any conclusion impossible in this case. The sedimentation time showed a decrease after UC exposure. Here, the low temperature sample showed the best results, as predicted. This is shown in the films. Note that the lowest part of Figure 14.12 (a) and 14.13 (a), and in the films, are tape and not a part of the sediment.

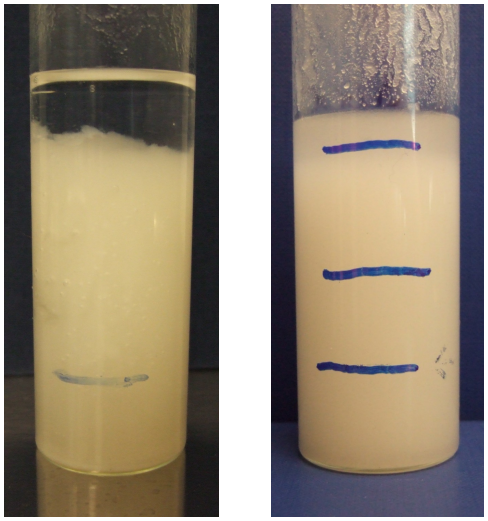

(a) (b)

Figure 14.10: (a) A liquid paraffin dispersion with AQAS. The blue mark shows the sedimentation height before exposing the sample to ultrasound. (b) Same sample as in (a), taken in solid paraffin condition. The lowest blue mark indicates the level of sedimentation without ultrasonic treatment, the upper mark after ultrasonic treatment, while the middle blue mark indicates the level of sedimentation after solidification and subsequent reheating, showing that the ultrasonic effect on the clay is reduced but not destroyed by solidification of the paraffin. (Any apparent divergency between the sample height and the blue marks in the two samples has to do with the solidification in (b) and the fact that some liquid was used from (b) for other experiments before the picture was taken.)

Figure 14.11: Samples of silicone oil and laponite RD. The left sample is without ultrasound treatment while the right sample is with ultrasound.

(a) (b) (c)

Figure 14.12: The width of the tubes are 1 cm and the depth 1 mm. (a) AQAS in silicone oil without ultrasonic exposure, (b) AQAS after ultrasonic exposure at 23 °C, (c) AQAS after ultrasonic exposure at 57 °C. Pictures taken immediately after injection in the tubes.

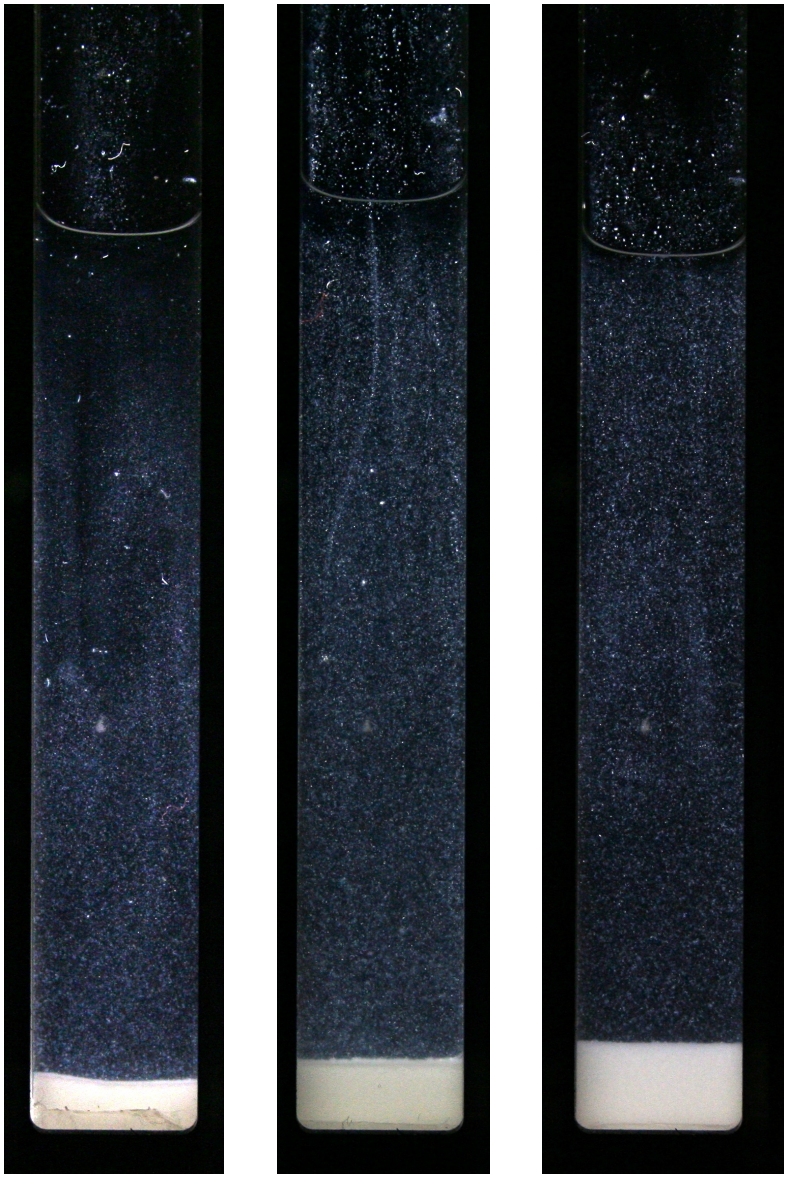

(a) (b) (c)

Figure 14.13: The width of the tubes are 1 cm and the depth 1 mm. (a) AQAS in silicone oil without ultrasonic exposure, (b) AQAS after ultrasonic exposure at 23 °C, (c) AQAS after ultrasonic exposure at 57 °C. Pictures taken after $\sim$ 24 hours.

An unexplained phenomenon is shown in Figure 14.14. After UC exposure, the AQAS suspension sometimes became gel-like and the particle phase seemed to pull upwards, making the clay float in the middle of the container. Unfortunately, the picture in Figure 14.14 does not show this strange behaviour very well. This was partly reproduceable, meaning that some samples showed this behaviour and some did not.

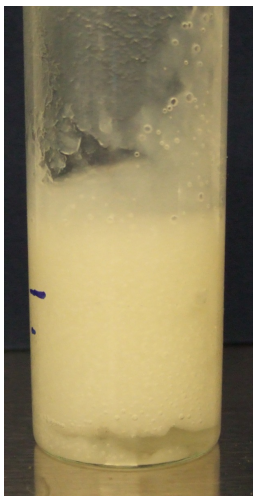

Figure 14.14: AQAS and liquid paraffin after ultrasonic treatment. The clay is gel-like and has pulled upwards. The clay seems to float in the middle of the container.

Chapter 15

X-ray Scattering

For almost all of the X-ray scans presented here, the center of the beam stop was erroneous. This was attempted compensated for when integrating, but the beam stop could not be perfectly adjusted. This may have caused a minor displacement of the curves, and the peaks to widen.

15.1 SAXS

The SAXS scans were integrated and plotted as shown in Figure 15.1. One scan of each sample type was included. The plot shows that there are no apparent difference in the scattering from the samples with and without field influence. The scattering from the AQAS samples are different than for the other clay species, probably indicating that the CTAB surface modification is not quite successful. The data was also fitted according to the counting time. The characteristic paraffin peak at $2\theta = 2.7°$ was calculated according to qquation 4.1, 4.2 and 4.3, and the d was found to be 16.36 nm. Bragg peaks from the scattering of the clay was not detected. The scattering data for the plot is shown in Figure 15.3 and Figure 15.4. The same scans were then plotted as function of χ, fitted according to the counting times. Little information can be found in Figure 15.2. The paraffin scan shows that the paraffin scatter too much compared to the clay, thus making the integration isotropic. It is alomst impossible to distinguish the different scans. The NiFH scans show anisotropic nature, possibly of fairly large particle size compared to the laponite clays. Unfortunately, the NiFH sample without ER structure has the same anisotropy as the two samples with chains.

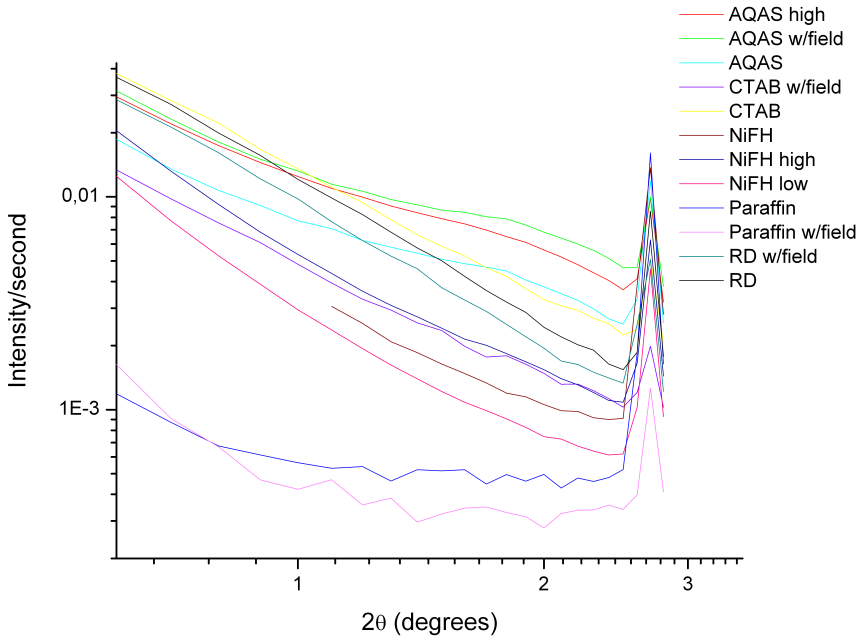

Figure 15.1: A SAXS 2θ vs. intensity plot for different species of clay frozen in paraffin. The data was fitted according to the counting times. The 2.7°-peak is paraffin Bragg scattering and corresponds to a layer distance $d = 16.36$ nm.

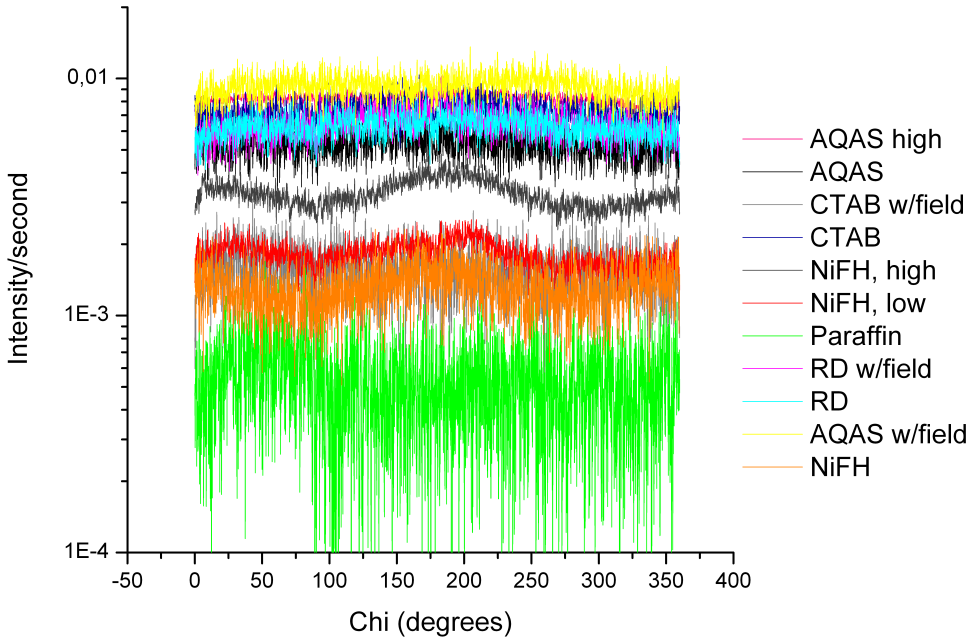

Figure 15.2: A SAXS χ vs. intensity plot for different species of clay frozen in paraffin.

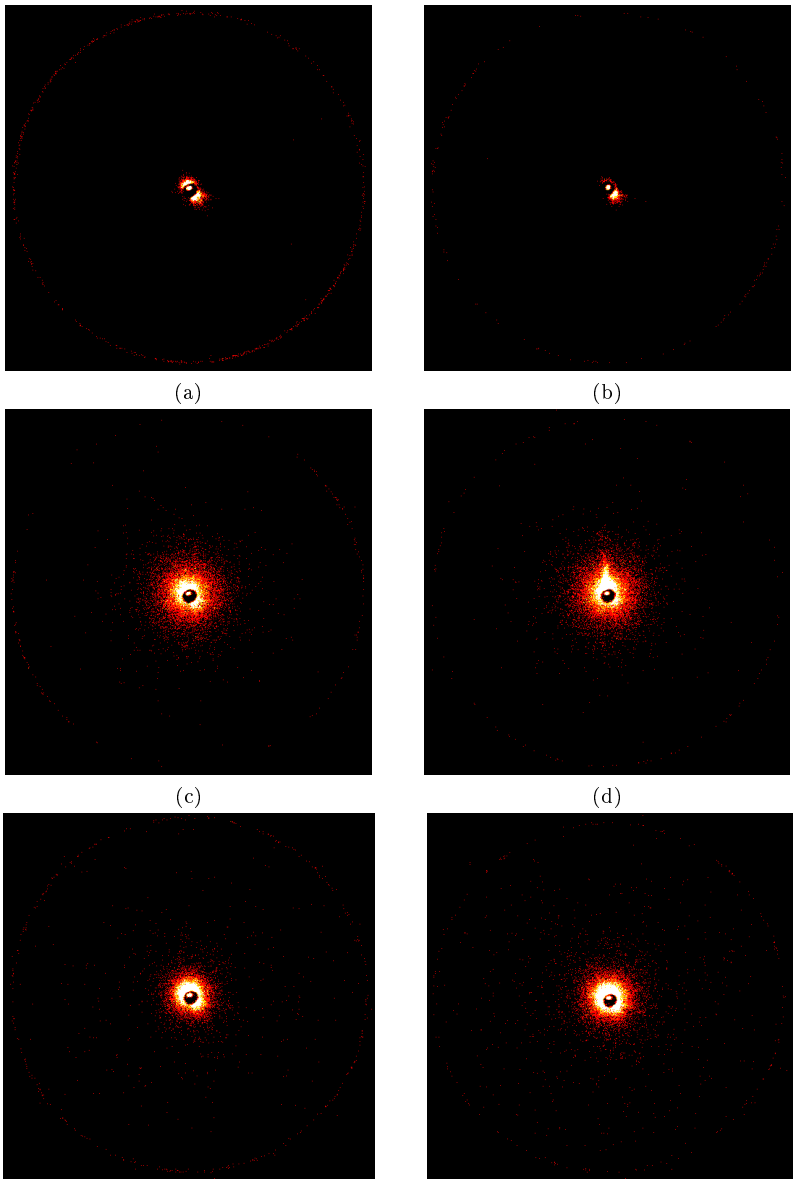

Figure 15.3: Scattering scans corresponding to Figure 15.1 and Figure 15.2. (a) Paraffin 240 s, (b) Paraffin with field 120 s, (c) Laponite RD without field 240 s, (d) Laponite RD with field 240 s, (e) AQAS without field 240 s, (f) AQAS with field 240 s.

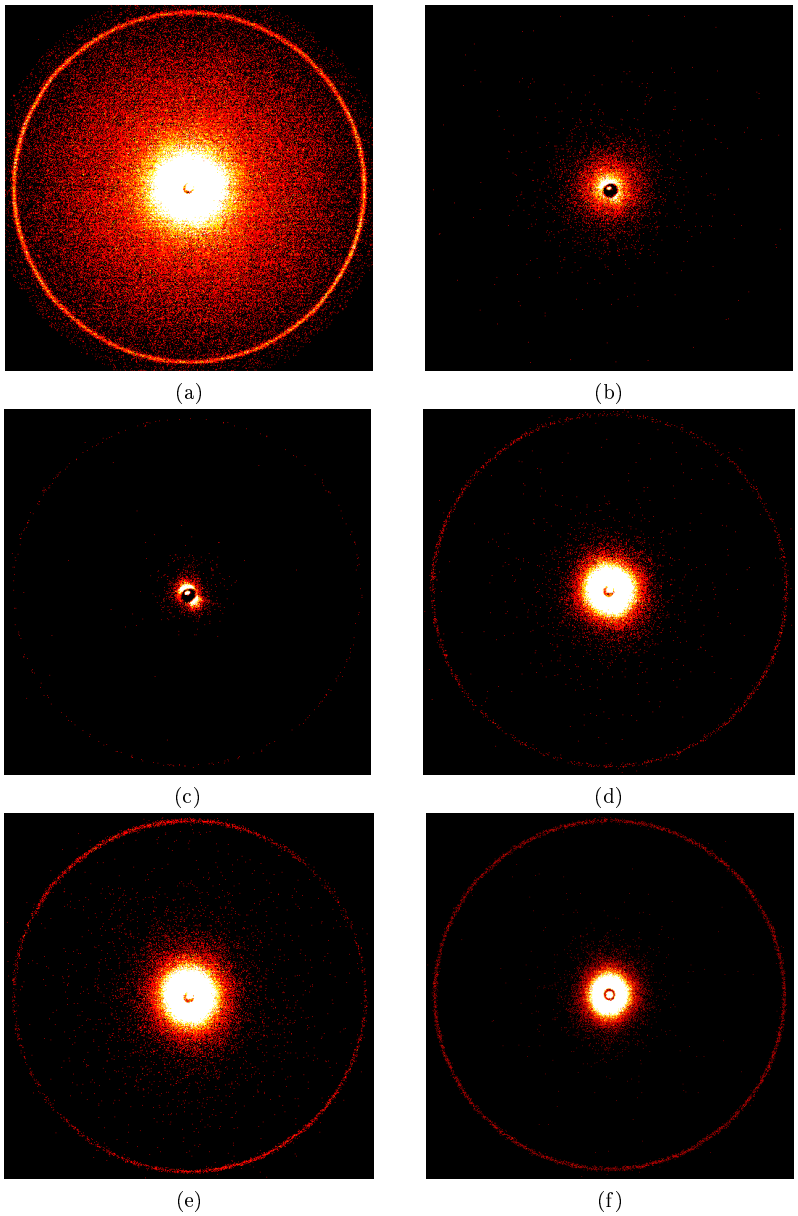

Figure 15.4: Scattering scans corresponding to Figure 15.1 and Figure 15.2. (a) AQAS with field, high concentration 2400 s, (b) CTAB without field 240 s, (c) CTAB with field 240 s, (d) NiFH with field, low concentration 1200 s, (e) NiFH with field, high concentration 1200 s, (f) NiFH without field 600 s.

The best scan of each of the two clay sample types investigated in silicone oil were then plotted as function of χ as shown in Figure 15.5. The scattering data corresponding to the plot in Figure 15.5, is shown in Figure 15.6. These scans are clearly anisotropic in nature and having their maxima at 0 and 180°, which should give the most scattering in the vertical direction. An investigation of Figure 15.6 confirms this, and it is also in agreement with a visual observation of the chain structure during the scans.

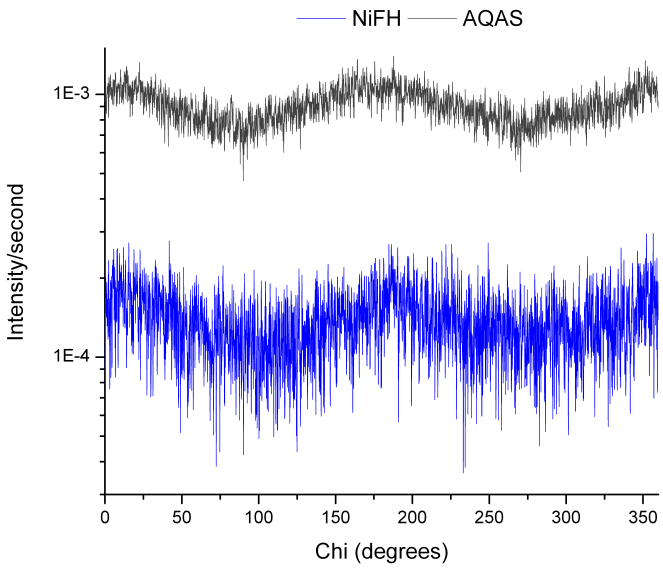

Figure 15.5: A SAXS χ vs. intensity plot for different species of clay in silicone oil.

15.2 WAXS

The WAXS scans were integrated and plotted as shown in Figure 15.7 and Figure 15.8. Figure 15.7 shows the χ dependence of the scattering. It is evident that little information can be extracted from this figure (not only bacause all scans were plotted in one figure), due to the paraffin scattering. The scans for AQAS were plotted again, shown in Figure 15.11, to closer examine possible differences. The anisotropy is somewhat clearer for the sample with ER structure, but not enough to conclude. The plots in Figure 15.8 shows the 2θ dependence of the scans. The two paraffin peaks were calculated, equation 4.3, to correspond to $d = 16.36$ nm and $d = 8.18$ nm. Any trace of Bragg peaks for clays were not found.

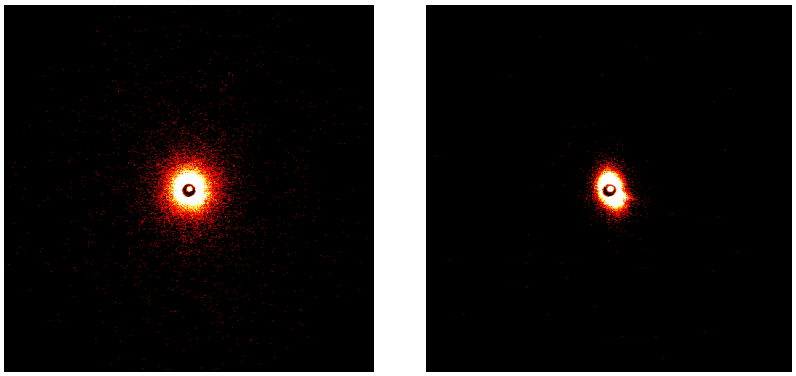

(a) (b)

Figure 15.6: Scattering data corresponding to Figure 15.5. (a) AQAS 2400 s and (b) NiFH 2400 s, in silicone oil. The field strength is 2 $\frac{\text{kV}}{\text{mm}}$ for both samples. The anisotropic scattering is observable, especially in (b).

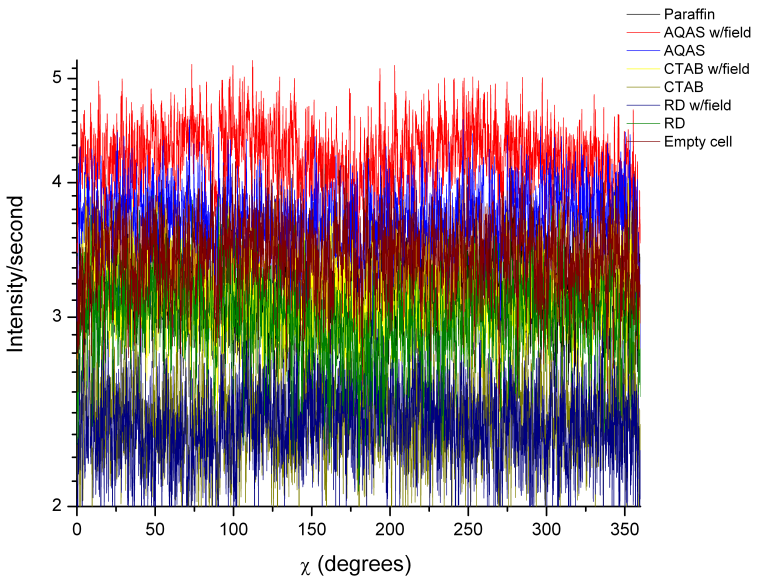

Figure 15.7: A WAXS χ vs. intensity plot for different species of clay in paraffin.

As decribed in chapter 10 different samples were investigated to observe the difference between the height and the width of the chains. An example of two different scans with AQAS is shown in Figure 15.13. The scattering seems quite similar. It was very difficult to verify the direction of the chains when the samples were placed in the sample holder, and the samples were not fixed

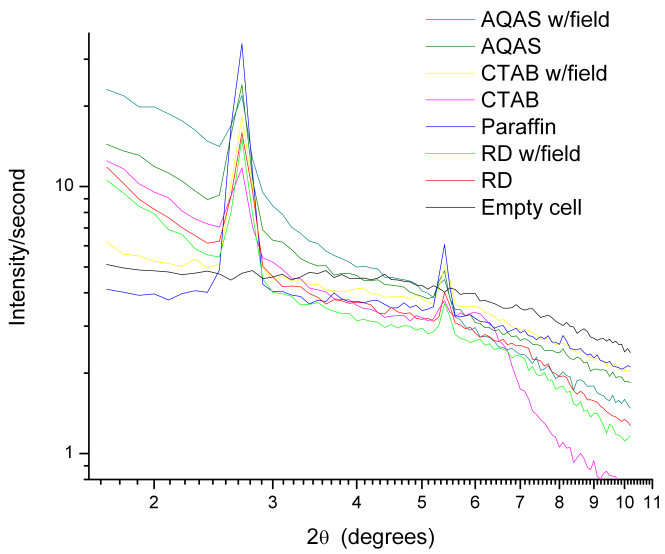

Figure 15.8: A WAXS 2θ vs. intensity plot for different species of clay in paraffin. The two peaks are paraffin Bragg scattering. The 2.7°-peak corresponds to layer distance $d = 16.36$ nm, while the 5.4°-peak corresponds to $d = 8.18$ nm.

very well, so a displacement of the chain orientation may have occured. The scattering noise from the paraffin shadows the clay scattering in any case, so differences are not observable.

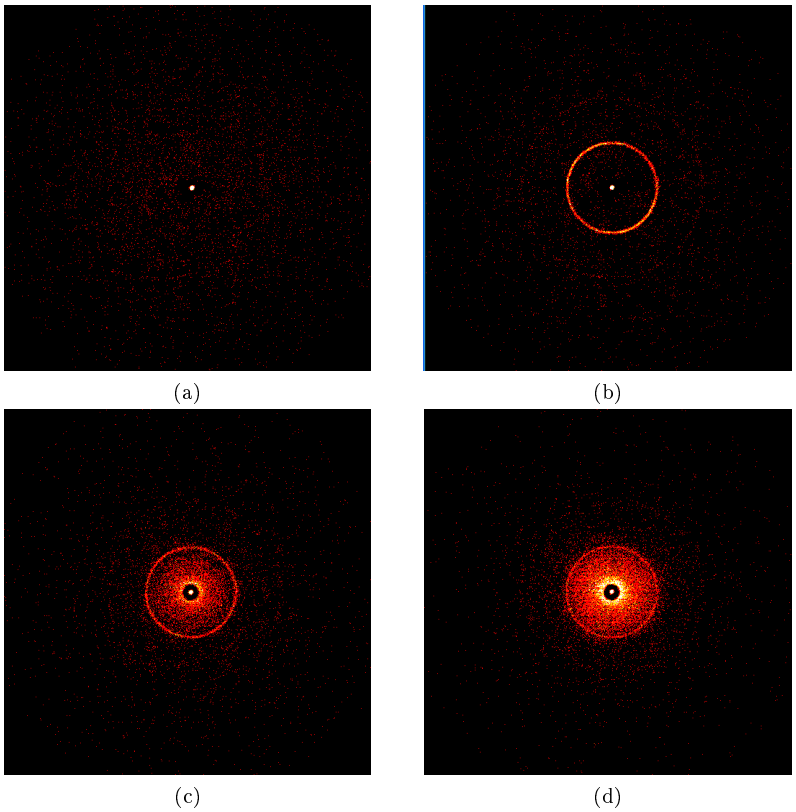

(a) (b)

(c) (d)

Figure 15.9: Scattering scans corresponding to Figure 15.7 and Figure 15.8. All scans are counted 120 s. (a) Empty cell, (b) Paraffin, (c) AQAS without field, (d) AQAS with field.

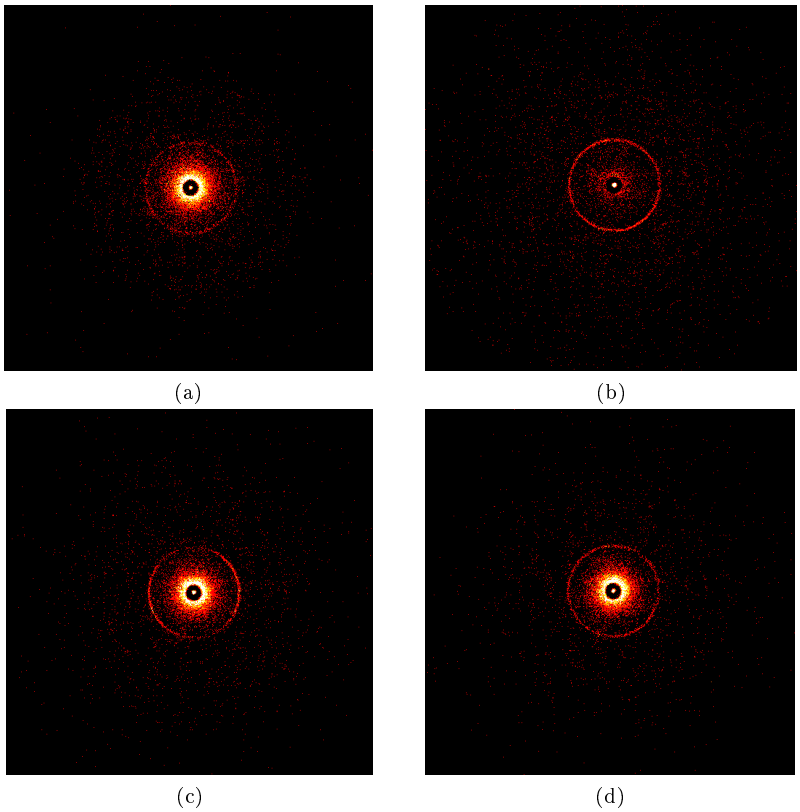

(a) (b)

(c) (d)

Figure 15.10: Scattering scans corresponding to Figure 15.7 and Figure 15.8. All scnas are counted 120 s. (a) CTAB without field, (b) CTAB with field, (c) RD without field, (d) RD with field.

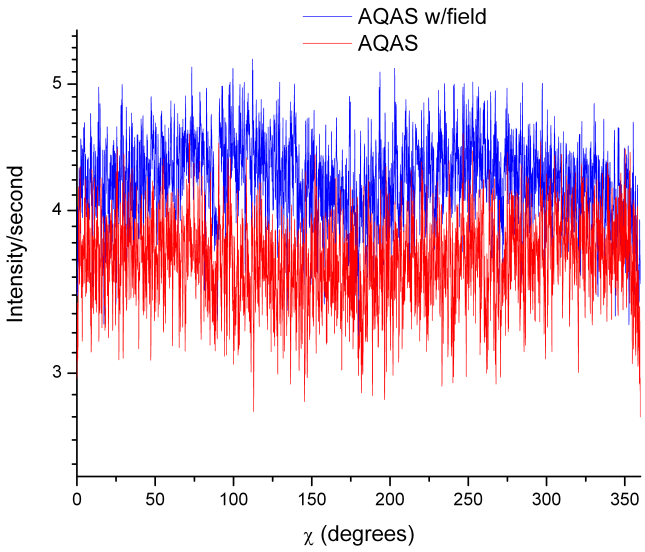

Figure 15.11: WAXS scans of AQAS with and without ER structure. The anisotropy is somewhat clearer for the sample with ER structure.

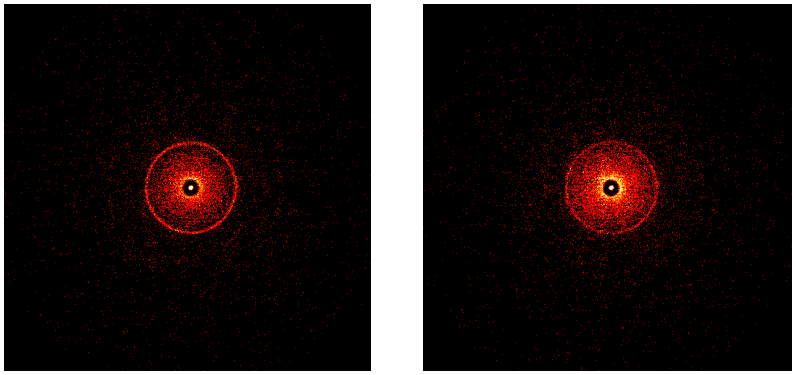

(a) (b)

Figure 15.12: Scattering data corresponding to Figure 15.11. (a) AQAS without field 240 s, (b) AQAS with field 240 s.

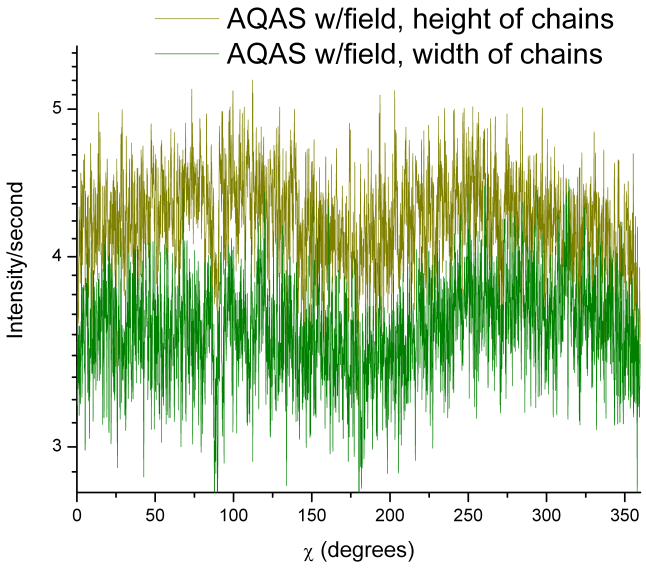

Figure 15.13: WAXS scans of two samples of AQAS in paraffin with different orientation. The scattering show no significally difference.

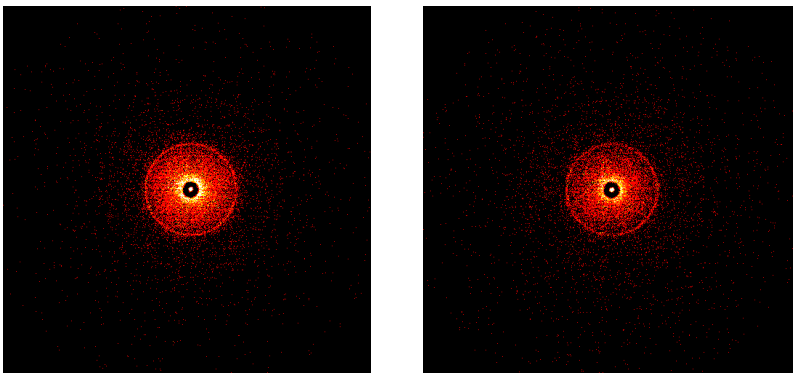

(a) (b)

Figure 15.14: Scattering data corresponding to Figure 15.13. (a) AQAS height of chains 240 s, (b) AQAS width of chains 240 s.

15.3 Field Effects on Paraffin

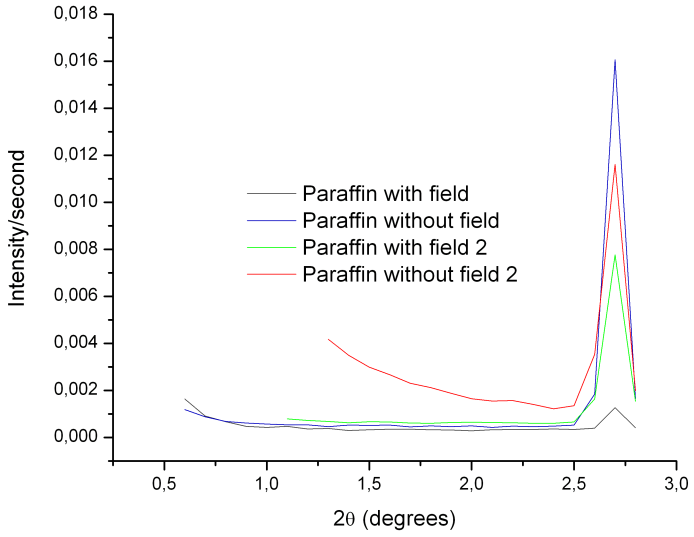

Figure 15.15: Four different scans of pure paraffin. Two scans of paraffin created in an electric field and two with no field applied.

Figure 15.15 illustrating an interesting effect that the electric field may have on the paraffin. All the four samples were made in the ER cell, but two of them without applying the voltage. As observable, the Bragg peak for the scans with no applied field is higher than the other two, which could mean that the presence of the electric field impairs the crystalline structure. Of course, the data material is not very extensive. However, this phenomenon occurs for all of the samples with paraffin, also when clay is dispersed in the paraffin. This can be seen when comparing the height of the peaks with and without field influence in Figure 15.1 and Figure 15.8. The scattering data for Figure 15.15 is shown in Figure 15.16.

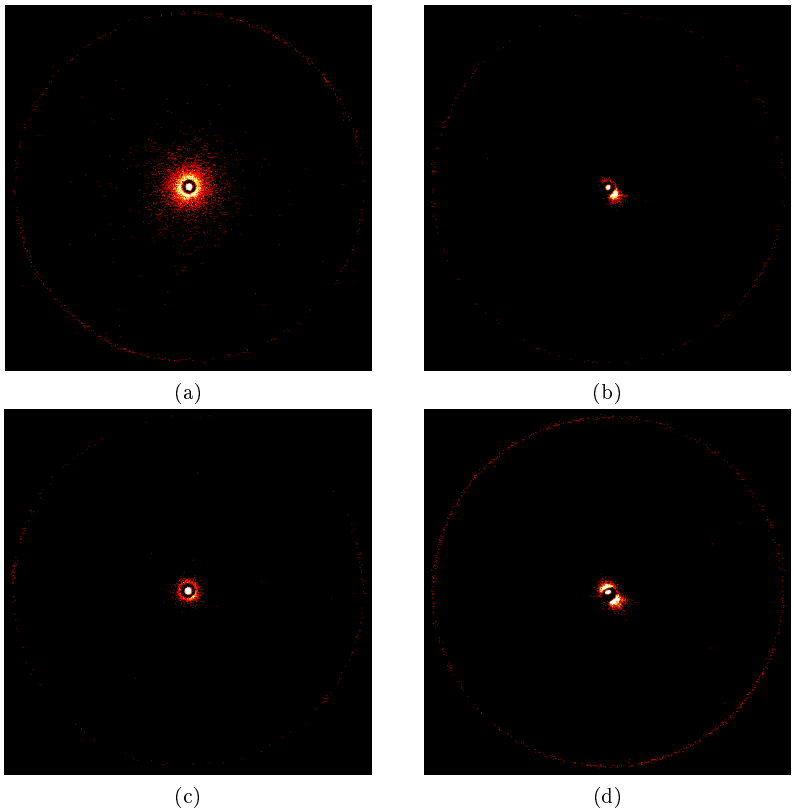

(a) (b)

(c) (d)

Figure 15.16: Scattering scans corresponding to Figure 15.15. (a) Paraffin with field 240 s, (b) Paraffin with field 120 s, (c) Paraffin without field 240 s, (d) Paraffin without field 240 s.

Chapter 16

Atomic Force Microscopy

Several pictures of AQAS in paraffin samples were taken, where visible chain structure were detected prior to the solidification of the paraffin during sample preparation. The pictures are shown in Figure 16.1 and Figure 16.2. All these pictures are taken of the same sample. Pictures of pure paraffin and an AQAS suspension without field influence were also taken.

The pictures were first considered indications of ER effect, i.e. chain formations. However, pictures presented by Zbik et al. [1] where paraffin wax surfaces are investigated, see Figure 16.3, shows a lack of difference in the pictures of AQAS and paraffin and the pictures of pure paraffin surfaces. A direct comparison can be made from Figure 16.3 and Figure 16.2 where the length scales are almost identical. The problem with the scans were figured out to be the rough surfaces of the samples. The surfaces were then tried to cut manually, to achieve a smooth surface. This may have romoved or destroyed the chains. To achieve good results, a precision instrument should be used. A computer controled cutter would be suitable instrument. An AFM study of electrorheological structure has probably never been carried out, and the work on this should be continued.

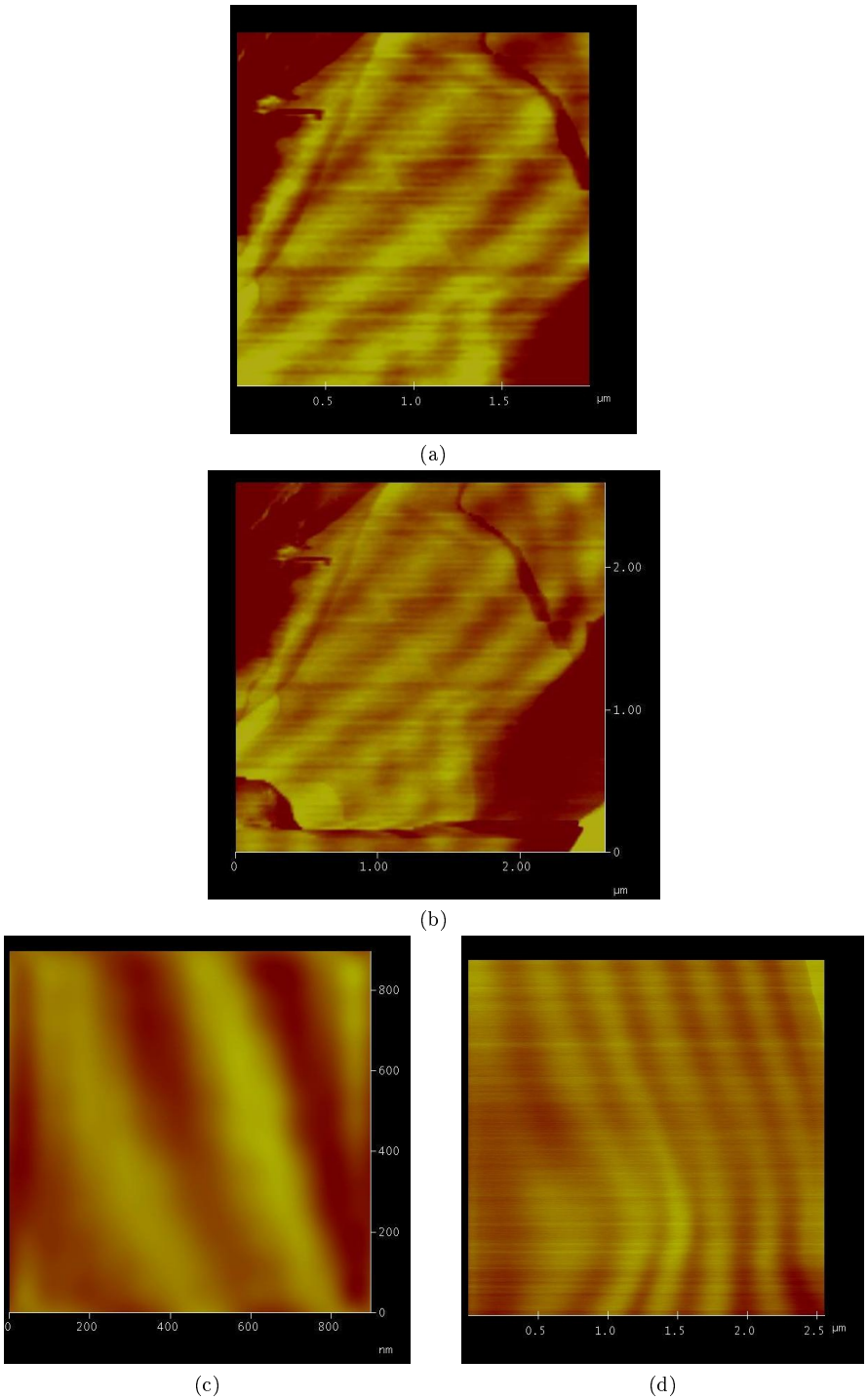

Figure 16.1: AFM pictures of AQAS frozen in paraffin at different length scale, indicated on the pictures.

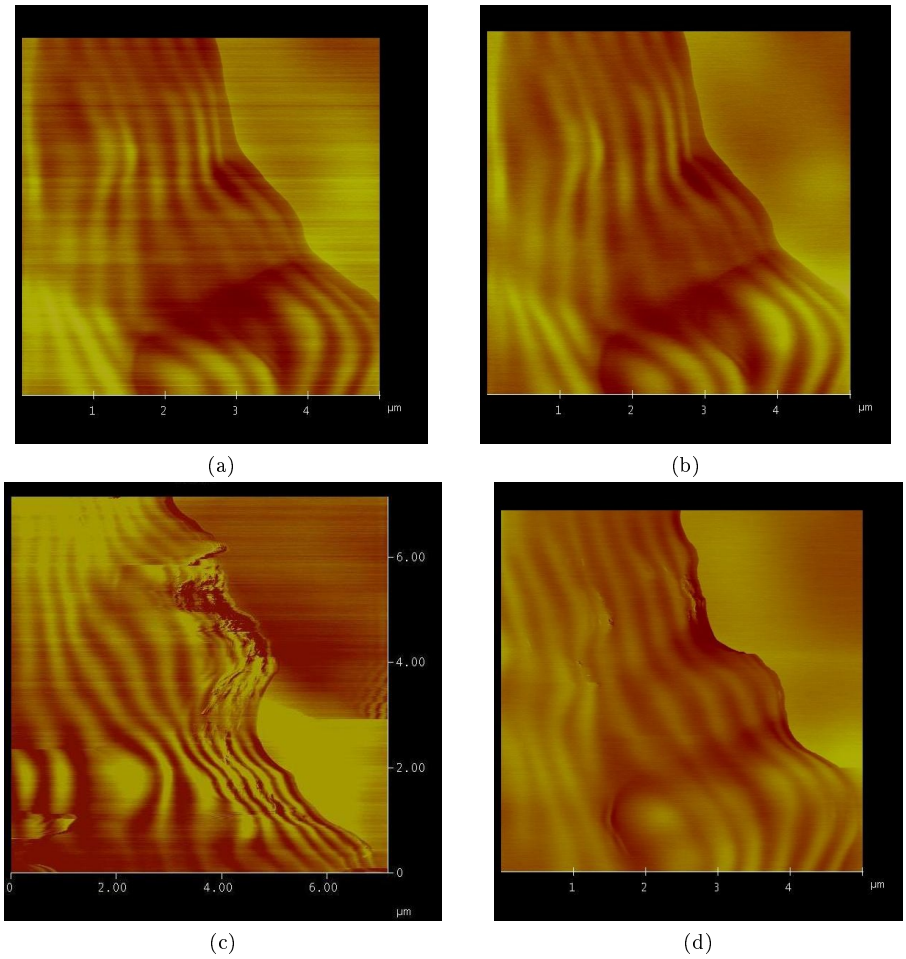

Figure 16.2: AFM pictures of AQAS frozen in paraffin at different length scale, indicated on the pictures.

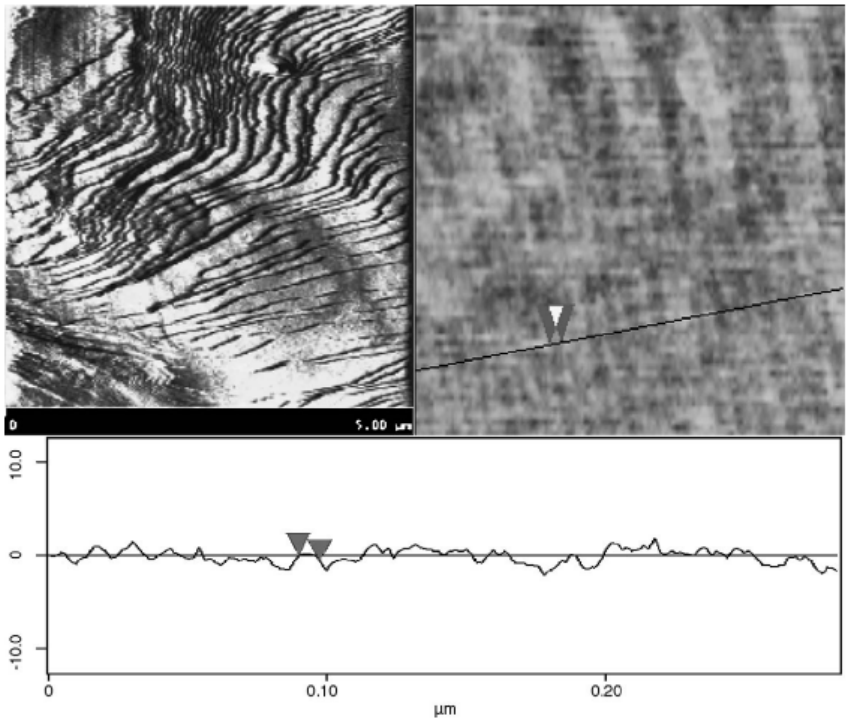

Figure 16.3: AFM pictures of paraffin surface in amplitude and height modes. Picture taken from Zbik et al. [1]

Chapter 17

Other Experiments And Analysis

17.1 Clay Concentration

When starting to work with the paraffin and clay, the intention was to have a clearly defined clay concentration in the samples, mostly for comparison. The fast sedimentation caused the necessity to visually choose at which height in the container the sample should be taken from, using a pipette. This fact resulted in an unpredictable clay concentration. There was some initial trial and error, as shown in Figure 17.1, where the consequence of chosing wrong concentration is illustrated. Neither of these samples were useful.

17.2 Paraffin as a Solvent

Initially the knowledge of the paraffin, its behaviour and properties, was limited. It was originally chosen based on some specific criteria. The material should be insulating to be suitable in ER experiments, and few other materials have a higher surface resistivity ($\rho \approx 10^{15}\ \Omega$). The material should also have its melting point just above room temperature to be able to work with the material both in liquid and soild state. The datasheet of the paraffin used sets the melting point in the intervall 46 - 48 °C. It was also of some importance that the chemical structure was simple, so the liquid carrier could be distinguished from the solvent. The paraffin consist approximately of 80 % straight alkanes, having a white partly transparent colour, thus a good choice. In addition, the paraffin was inexpensive, easy accessible and non-toxic. Figure 9.2 shows that the laponite chains are clearly visible when the paraffin is liquid. The pictures

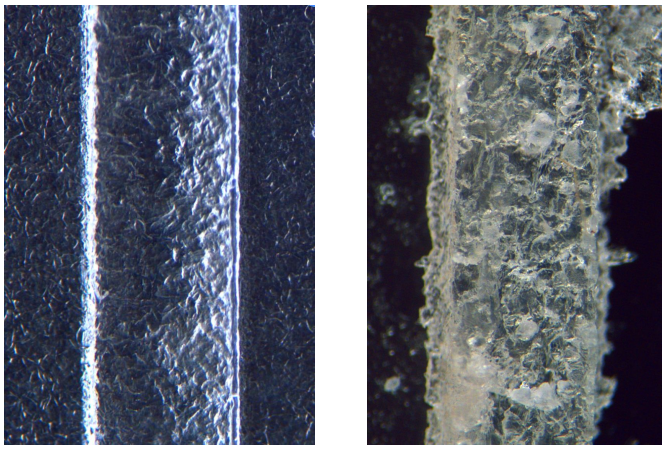

(a) (b)

Figure 17.1: (a): Experiment with too low concentration of clay. Possible chains are not observable., (b): Experiment with too high concentration of clay. The sample is pasty and contains no evident chains.

in section 13.1 show that the chains are also visible in solid paraffin.

After thorough work with paraffin some disadvantageous properties were revealed. Primarily, there were considerable problems with sedimentation as explained in chapter 14. In addition to that, the solid paraffin was perhaps too soft, especially when trying to cut the sample. This could only be done with considerable difficulty, and the risk of destroying the sample was impending. Paraffin samples were also difficult to handle in the AFM. Great care had to be shown in mounting the sample in the AFM to keep the chain structure intact. Soft materials also require the use of the tapping mode, which is a slow probe compared to its alternatives. The softness was at the same time an obstacle in the X-ray experiments where the sample had a tendency to bend and deform so that the chain orientation in the sample was hard to determine. This also has to do with the fact that the colour of the chains are quite similar to the paraffin colour, as shown in Figure 13.5 (a). The scattering from the paraffin was also of such a character that many of the scans were of little value because of noise from the paraffin scattering. Finally, the paraffin was hard to remove from the glass during the sample preparation and in particular from the cell, due to a very sticky surface. The problem with the glass surface was solved by using a plastic film on top of it, but the problem of removing the sample from the cell remained an obstacle. Dr. Boaxiang Wang created a new cell based on the experience with the old. This new cell had a wider gap, of 1.5 mm, and was not as fragile as the old. This cell could probably solve the described cell problems, but unfortunately, it was not available for use in time for the described experiments.

17.3 Electrorheological Measurements in the Rheometer

To investigate the ER effect for the different clays, a static yield stress test was performed. An electric field was applied to the samples for 5 min, then an increasing shear stress in steps of 0.5 Pa was imposed on the samples. The yield stress was taken at the stress where a sudden increase in the shear rate appeared.

In Figure 17.2 the yield stress for laponite RD and AQAS in paraffin is shown. Figure 17.3 show the equivalent results for clay in silicone oil.

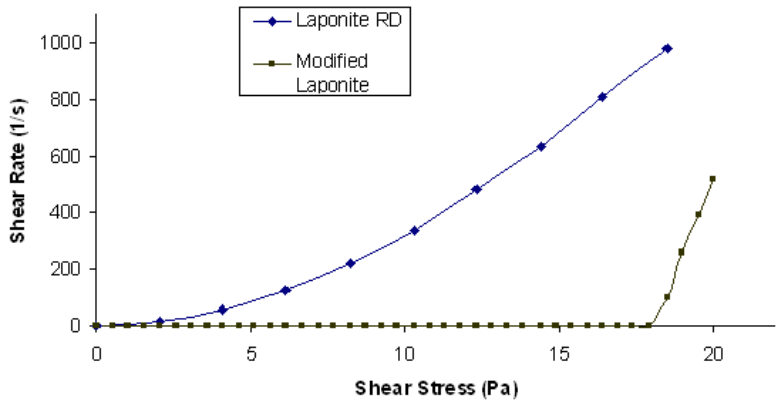

Figure 17.2: The yield stress of two different clays in paraffin. The RD experiment is performed at 60 °C, while the AQAS experiment at 52 °C.

Comparing Figure 17.2 and Figure 17.3 show that the ER effect is apparent for the AQAS in paraffin and also stronger than it is when solved in oil, a static yield stress of approximately 17 Pa compared to 6 Pa. The test with laponite RD in paraffin shows no ER effect at all. Figure 17.2 shows that the shear rate increases immediately, indicating no ER effect present, most likely because the particles has sedimented before the measurements, see section 14.1.

The CTAB showed a much weaker static yield stress, approximately 16 Pa, compared with laponite RD at the same concentration, which has 37.5 Pa[1]. This can be explained by the fact that the relative laponite concentration is lower for the CTAB than for the laponite RD, but also that the CTAB surfactant has changed the surface properties of the laponite RD particles.

[1] Found in an experiment by Børge Aune Schjelderupsen

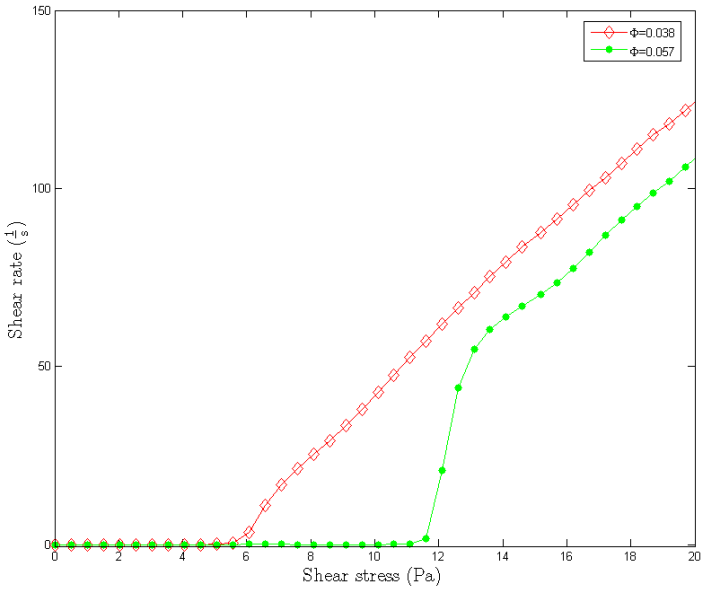

Figure 17.3: Yield stress in silicone oil for AQAS at different volume fractions of $\Phi = 0.038$ and $\Phi = 0.057$. $\Phi = 0.038$ correspond to the volume fraction used in Figure 17.2. (Experiment performed by Børge Aune Schjelderupsen.)

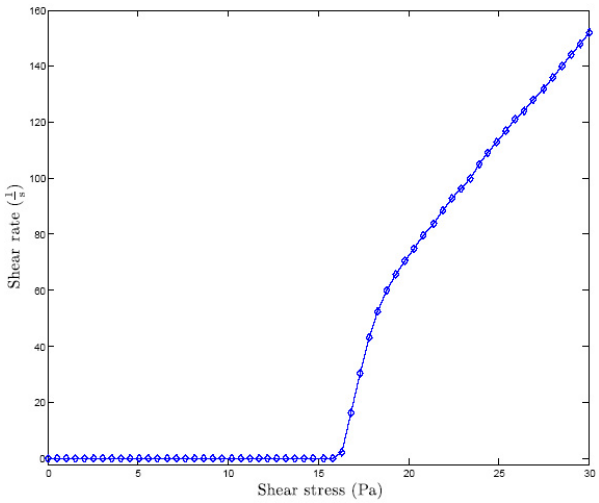

Figure 17.4: Static yield stress measurement of CTAB ($\Phi = 0.2$) in 0.89 $\frac{\text{kV}}{\text{mm}}$.

17.4 Samples in Magnetic Field

An AQAS suspension, equivalent to the ones described in section 12.2.2, where tested in a magnetic field using the magnet shown in Figure 17.5. These experiments has little interdependence with the other experiments described, and were thus not analysed very deeply and no conclusions were drawn. Nevertheless, some results are presented. A more thorough study of this could be a topic for further studies. These experiments were performed in collaboration with Nils Ivar Ringdal with his experimental setup containing crossed polarizers.

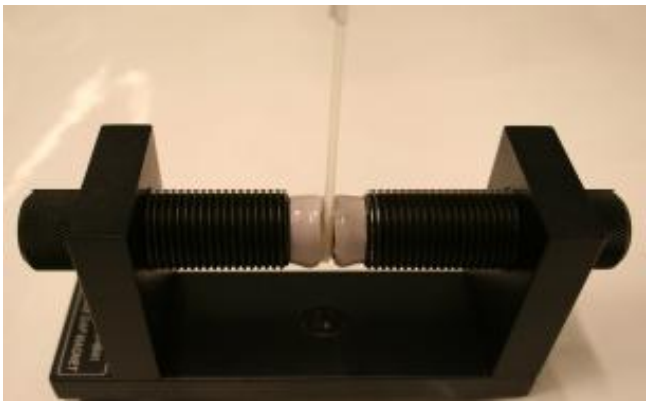

Figure 17.5: Experimental setup for samples in magnetic field. The field strength is 1 T when the gap is as shown in the figure.

In Figure 17.6 (a), the sediment has been exposed to the magnetic field, and the particles tend to arrange to the field. In Figure 17.6 (b) the upper phase is exposed to the magnetic field and the particles are clearly arranged more or less perpendicular to the field near the magnet area. The black spot indicates where the magnet was placed. The fact that the spot is black, i.e. no transmission in the crossed polarizers, indicates that the magnet causes the particles to form an isotropic arrangement. Figure 17.7 shows a series of pictures after the sample had been exposed to the magnetic field for approximately 15 days. The three pictures are taken within a few minutes after the sample was removed from the magnet. Note the black spots on the upper phase still present, the areas where the magnet has previously been placed.

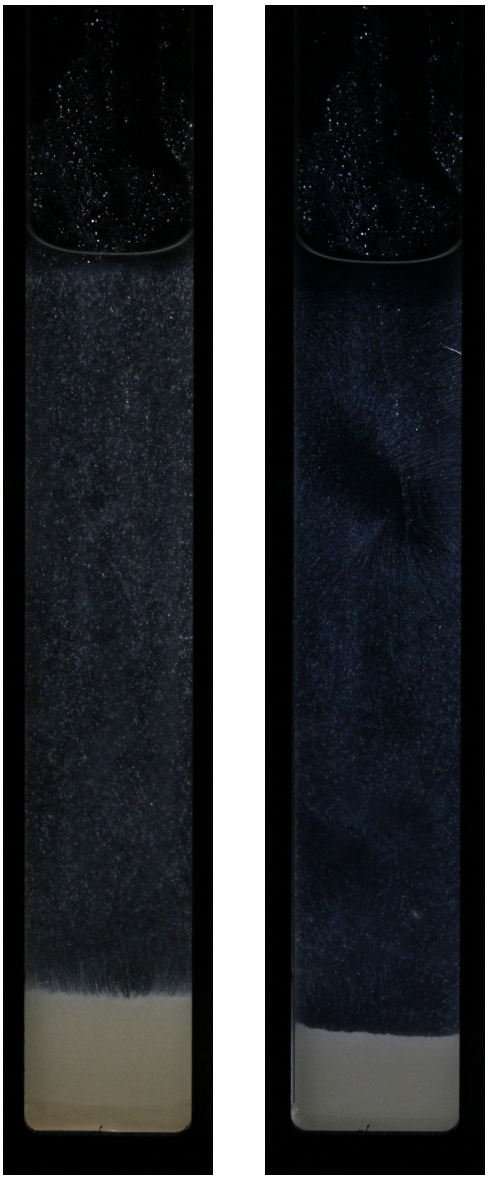

(a) (b)

Figure 17.6: AQAS sample in silicone oil after exposure to magnetic field. The tubes are 1 cm wide and 1 mm thick.

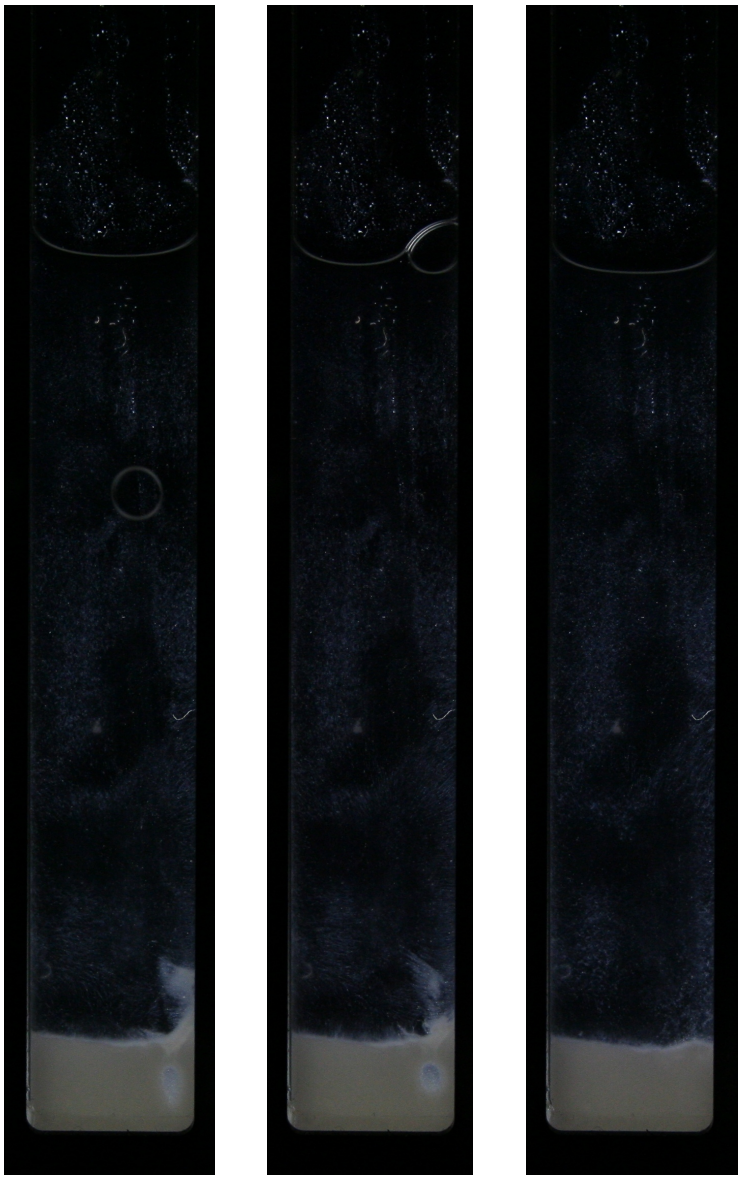

(a) (b) (c)

Figure 17.7: AQAS sample in silicone oil after exposure to magnetic field for approximately two weeks. The tubes are 1 cm wide and 1 mm thick.

Part V

Conclusions

Chapter 18

Conclusions

This has been an experimental study of the structure and resulting electrorheological behaviour of clays dispersed in melted paraffin wax or silicone oil. The conclusions on the different experiments are split up into the sections below.

18.1 Paraffin

The melted paraffin proved to be a suitable solvent for ER performance. The paraffin wax was also appropriate for visual observation of the chain structure. However, paraffin is most likely not a suitable liquid for ER applications, since the clay sedimentation rate is high due to low viscosity and a high operating temperature, which are correlated. Nevertheless, rheometer experiments with AQAS shows that ER effect in paraffin is present and strong. In X-ray scattering experiments, the dominating scattering from the paraffin overshadows the scattering from the clay, and paraffin is thus unsuitable with the equipment used. An alternative to paraffin, or a supplement, should be found.

18.2 Lipophilic Clays

The attempt to modify the laponite RD with CTAB was partly successful. The sedimentation rate in silicone oil proved lower than for equivalent experiments with normal laponite RD. This was indicated both rheologically and visually. As expected, the ER effect was weaker than for untreated laponite RD, since the relative clay concentration is lower and the surface properties are changed with the use of CTAB. A comparison between the ER effect of AQAS and CTAB showed only a slight difference. A questionable aspect with the CTAB was the time-consuming treatment procedure, where only small amounts of finished

clay were produced in each session. In addition, the grinding method used was insufficient, since large particles were present. Dr. Wang tried a different approach in the surface modification based on a method by Ogawa et al. [48]. The main differences were the use of water instead of the ethanol and the lower drying temperature. This method showed much better results. However, even if the surface modification method should prove sucessful, the industry fabricated clay AQAS showed equal or superior behaviour in all experiments, thus making the CTAB modification redundant.

18.3 Light Microscopy

The microscope technique proved suitable to take pictures of chain structures and also suitable for recording of films. Pictures of laponite RD in paraffin were taken between crossed polarizers, where birefringence and anisotropy were evident. The work with birefringence was not very extensive and should be investigated further.

18.4 Sedimentation

The reduction of the sedimentation rate, i.e. the total sedimentation, for AQAS in liquid paraffin was significant. The memory of ultrasound treatment was also present to some extent in the same samples after solidification and reheating of the paraffin. Similar tests with silicone oil showed a slight improvement. Ultrasound was also tested with respect to sedimentation times. It was found that AQAS samples in silicone oil sediments slowed after ultrasound treatment and that the effect was strongest for low temperature ultrasound treatment. Some unexplained features of the sedimentation were also found. The theoretical background on sedimentation was limited, and observations were not always easy to explain. A thorough study of sedimenation of ER suspension and sedimenation theory provides an interesting topic for further study.

18.5 X-ray Scattering

The X-ray scattering experiments with paraffin were unsuccessful, due to dominating paraffin scattering, as mentioned in section 18.1. The scattering data from the oil suspension showed anisotropic pattern, indicating a direction preference of the clay particles and thus present ER effect. Synchrotron scattering may provide results for paraffin samples as well.

18.6 AFM

No evidence for ER structure was observed using AFM. This propbably has to do with the roughness of the sample surfaces. To cut the samples in order to smoothen the surface without ruining or removing the clay structure, proved difficult. A computer controlled cutting technique may provide a solution to the problem, and further work should yield good results.

Bibliography

[1] M. Zbik R.G. Horn, N. Shaw. AFM study of paraffin wax surfaces. *Colloids and Surfaces A: Physicochemical and Engineering Aspects*, 287, 2006.

[2] T. Hao. Electrorheological fluids. *Advanced Materials*, 13(24), 2001.

[3] Weijia Wen P. Sheng, Xianxiang Huang. Particle size scaling of the giant electrorheological effect. *Applied Physics Letters*, 85(2), 2004.

[4] K. Walters H.A. Barnes, J.F. Hutton. *An Introduction to Rheology*. Elsevier, 1989.

[5] W.M. Winslow. *J. Appl. Phys.*, 20, 1949.

[6] X. Huang. *Theoretical Study of Electrorheological Fluids*. PhD thesis, Hong Kong University of Science and Technology, 2004.

[7] X.Y. Xu K.Q. Lu Y.C. Lan, S.Q. Men. Experimental study of dielectric constant influence on electrorheological effect. *J.Phys.D: Appl.Phys.*, 33: 1239–1243, 2000.

[8] T. Hao. Electrorheological suspensions. *Advances in Colloid and Interface Science*, 97:1–35, 2002.

[9] K. Suh J. Jun. Preparation and electrorheological characterization of suspensions of poly(urethane acrylate)/clay nanocomposite particles. *J. of Appl. Polymer Science*, 90:458–464, 2003.

[10] D.J. Klingenberg M. Parthasarathy. Electrorheology: mechanisms and models. *Materials Science and Engineering*, R17:57–103, 1996.

[11] K.P.S. Parmar. *Oil dispersions of nano-layered silicates in an external electric field: An experimental study*. PhD thesis, NTNU, 2006.

[12] A. Acrivos B. Khusid. Effects of conductivity in electric-field-induced aggregation in electrorheological fluids. *Phys. Rev. E*, 52:1669, 1995.

[13] Derivation of flow rate equation for bingham-fluids. http://www-tu-dresden.de/mwilr/lampe/bingham/bingeng.htm, December 4th 2006.

[14] Materials Digital Library (MatDL). http://matdl.org/matdlwiki/index.php/Surfactant, June 18th 2007.

[15] Water Quality Association (WQA). http://www.wqa.org/glossary.cfm?gl=1354, June 18th 2007.

[16] IUPAC Compendium of Chemical Terminology. http://goldbook.iupac.org/L03572.html, June 2nd 2007.

[17] University of Maryland Clark School of Engineering. `http://www.isr.umd.edu/CELS/research/watersim/guidance/educational\%20module/ion_exchange1.htm`, November 21th 2006.

[18] B. Velde. *Origin and Mineralogy of Clays, Clays and the Environment.* Springer, 1995.

[19] G. Strobl. *Condensed Matter Physics.* Springer, 2004.

[20] D. McMorrow J. Als-Nielsen. *Elements of Modern X-ray Physics.* Wiley, 2001.

[21] Mount Holyoke College Massachusetts. http://www.mtholyoke.edu/ mlyount/MySites/ForensicSpectroscopy/Vocab.html, June 22th 2007.

[22] High-Tech Digital. http://www.high-techdigital.com/integration/optics_t_1.htm, June 22th 2007.

[23] M. Young. *Optics and Lasers.* Springer, 1992.

[24] J.R. Meyer-Arendt. *Introduction to Classical and Modern Optics.* Prentice-Hall, 1995.

[25] Case Western Reserve University. http://plc.cwru.edu/tutorial/enhanced/files/lc/light/light.htm, June 22th 2007.

[26] *Megapixel FireWire Camera User's Manual PL-A6XX*, 2002.

[27] Kalz Brandschutz Elektrotechnik. http://www.kalz-online.de/PeakTech4370.pdf, May 30th 2007.

[28] G. Heinemann Ultraschall und Labortechnik. http://www.gheinemann.de/5510.jpg, May 30th 2007.

[29] Vecco Metrology Group Digital Instruments. Scanning Probe Microscopy Training Notebook Version 3.0, 2000.

[30] *Bruker AXS NanoSTAR SAXS System User Manual Vol. 2*, 2004.

[31] J.O. Fossum. Physical phenomena in clays. *Physica A*, 1999.

[32] G. Lagaly F. Bergaya, B. K. G. Theng. *Handbook in Clay Science.* Elsevier, 2006.

[33] E. DiMasi K.J. Måløy S.B. Lutnæs G. J. da Silva, J.O. Fossum. Synchrotron x-ray scattering studies of water intercalation in a layered synthetic silicate. *Phys. Review E*, 2002.

[34] T.J. Schröder P.D. Kaviratna, P.D. Pinnavaia. Dielectric properties of smectic clays. *J. Phys.Chem. Solids*, 1996.

[35] Encyclopædia Britannica. Silicate layer: 1:1 and 2:1 structures. [Art] http://www.britannica.com/eb/art-2439, June 22th 2007.

[36] Mineralogy database. http://webmineral.com/data/Hectorite.shtml, May 29th 2007.

[37] T. Gog C. Venkatarman E. DiMasi, J.O. Fossum. Orientational order in gravity dispersed clay colloids: A synchrotron x-ray scattering study of Na-fluorohectorite suspensions. *Phys. Review E*, 2001.

[38] Rockwood. Laponite - the performance enhancer. www.laponite.com, October 23th 2006.

[39] *Aschehougs koversasjonsleksikon*, volume 15, page 346. Aschehoug, 1974.

[40] IGI Wax. http://www.igiwax.com/resource/Wax_Overview, November 28th 2006.

[41] Tables of Physical & Chemical Constants Kaye & Laby. http://www.kayelaby.npl.co.uk, June 2nd 2007.

[42] S. V. Kharlamov et al. Aggregation in a Mixture of Cetyltrimethylammonium Bromide and Polyoxyethylene 600 Monolaurate Solutions. *Colloid Journal*, 68(**4**):550–557, 2006.

[43] H. Conrad C.W. Wu. The Temperature Dependence of the Conductivity of Silicone Oil and Related Electrorheology of Suspensions Containing Zeolite Particles. *J. Appl. Phys.*, (**31**):3403, 1998.

[44] K. Franklin J.S. van Duijneveldt E.S.H. Leach, A. Hopkinson. Nonaqueous suspensions of laponite and montmorillonite. *Langmuir*, 21:3821–3830, 2005.

[45] J.K. Thomas T. Nakamura. Formation of surfactant double layers on laponite clay colloids. *Langmuir*, 3:234–239, 1987.

[46] S Men K. Lu Y. Lan, X. Xu. Orientation of particles in an electrorheological fluid under an electric field. *Physical review E*, 60(24):4436–4439, 1999.

[47] J. A. Powell. The mechanical properties of an electrorheological fluid under oscillatory dynamic loadning. *Smart Matter.Struct.*, 2:217–231, 1993.

[48] K. Kuroda M. Ogawa. Preparation of inorganic-organic nanocomposites through
intercalation of organoammonium ions into layered silicates. *Bull. Chem. Soc. Jpn.*, 70, 1997.

Appendix A

DVD Index

ER films:

V1: Showing a dispersion of Laponite RD treated with ultrasound.

- V_T occurs after approximately 12 s. Notice the absence of visible chains. (First chain after 62 s.)
- 84-85 s. Reorganizing of the chains. Formation of columns. It seems like the large particle triggers the creation of the chain.
- 92 s. Showing what happens after the voltage is turned off. The flux has once more a preference of flowing down the gap, similar to $t \leq 12$ s.

V2: Showing a dispersion of Laponite RD treated with ultrasound.

- V_T occurs after approximately 9 s.
- The voltage starts at 0 V and increases continuously up to approximately 3 kV.
- The film illustrates the creation and development of chains and subsequently columns.

V3: Showing a dispersion of Laponite RD.

- Voltage is turned on to a constant voltage 2 kV.
- Columns appears almost immediately after the voltage is turned on. Notice the difference in the column development compared to other films, e.g. V2. The columns are created by growth form unattached particles, not by merging of chains.

V4: Showing a dispersion of AQAS.

- V_T occurs after approximately 17 s.

- Voltage are turned off after approximately 50 s.

V5: Showing a dispersion of AQAS.

- Voltage is turned on to a constant voltage 2 kV.
- A very small amount of oil is used, giving an almost two-dimensional suspension.

Sedimentation films:

These films should be seen simultaneously to be able to compare them to each other.

V6: Sedimentation of AQAS for approximately 24 hours.

V7: Sedimentation of AQAS treated with ultrasound at 23 °C for approximately 24 hours.

V8: Sedimentation of AQAS treated with ultrasound at 57 °C for approximately 24 hours.